Improvement of Electrode/Electrolyte Interfaces in High-Voltage Spinel Lithium-Ion Batteries by Using Glutaric Anhydride as Electrolyte Additive

H. Bouayad, Z. Wang, Nicolas Dupre, Rémi Dedryvère, Dominique Foix, S. Franger, J.-F. Martin, L. Boutafa, S. Patoux, Danielle Gonbeau, et al.

Improvement of Electrode/Electrolyte Interfaces in High-Voltage Spinel Lithium-Ion Batteries by Using Glutaric Anhydride as Electrolyte Additive

H. Bouayad [1], Z. Wang [2], N. Dupré [2,5,6,*], R. Dedryvère [1,5,6,*], D. Foix [1,5,6], S. Franger [3], J.-F. Martin [4], L. Boutafa [4], S. Patoux [4], D. Gonbeau [1,5,6], D. Guyomard [2,5,6]

[1] *IPREM/ECP, CNRS UMR 5254, University of Pau, France*
[2] *Institut des Matériaux Jean Rouxel, CNRS UMR 6502, Université de Nantes, France*
[3] *ICMMO/EPCES, CNRS UMR 8182, University Paris Sud, Orsay, France*
[4] *LITEN, CEA, Grenoble, France*
[5] *Alistore - European Research Institute, 33 rue Saint-Leu, 80039 Amiens cedex, France*
[6] *Réseau sur le Stockage Electrochimique de l'Energie (RS2E), FR CNRS 3459, France*

Abstract:

High-voltage spinel oxides combined with $Li_4Ti_5O_{12}$ result in 3V Li-ion batteries with a high power capability, but electrochemical performances are limited by electrode/electrolyte interfacial reactivity at high potential. We have investigated glutaric anhydride (GA) as electrolyte additive to improve the performances of $LiNi_{0.4}Mn_{1.6}O_4/Li_4Ti_5O_{12}$ cells. We showed that GA efficiently reduces both the capacity fading upon cycling and the self-discharge. From X-ray Photoelectron Spectroscopy (XPS), Nuclear Magnetic Resonance (NMR) and Electrochemical Impedance spectroscopy (EIS) measurements, we showed that GA reduces salt ($LiPF_6$) degradation. Addition of 2% GA in the electrolyte results in a passivation film at the surface of both electrodes, which is mainly composed of organic compounds resulting from degradation of GA. The film is much thicker but less resistive due to a better ionic conductivity, and behaves like a Polymer Electrolyte Interface.

Keywords: Li-ion batteries, high voltage spinels, $Li_4Ti_5O_{12}$, electrolyte additives, interfaces, XPS, NMR, impedance

* corresponding authors: nicolas.dupre@cnrs-imn.fr, remi.dedryvere@univ-pau.fr

1. Introduction

The need for portable source of energy becomes increasingly important with the technology development as it can be used in a wide variety of applications ranging from robotization, electric or hybrid vehicles, power tools, biological and energy storage. Hence, it is necessary to develop low-cost, safe, rechargeable batteries of high voltage, capacity and rate capability.[1] Lithium ion batteries are today the most promising power source of the portable electronic devices.

Compared with lead-acid and Nickel-MH batteries, a lithium battery has higher power and energy, making it appropriate for cell phones and lap-top computers. However, safety, energy, power and cost are still issues for its application in electric vehicles. For these large size batteries, safety is in particular a crucial issue and it is still a weak point of the Li-ion technology that must be resolved in a near future. In the current Li-ion batteries, carbon negative electrodes raise a safety problem because metallic lithium may be plated at the electrode surface due to the low Li ions intercalation potential during a fast charge. From that point of view, spinel lithium titanate $Li_4Ti_5O_{12}$ (named LTO hereafter) is a safer negative electrode material due to its higher Li intercalation potential and could replace carbon or graphitic negative electrodes.[2,3,4] As a positive counter electrode, olivine $LiFePO_4$ is a promising candidate due to its safety, environmental friendliness and low cost but the working voltage of a $LiFePO_4$/LTO battery is only 1.9V. In order to meet desired requirements in terms of voltage and then power and energy density, one good solution is to use high voltage spinels, such as $LiMn_{2-x}M_xO_4$, as the positive electrode material in the LTO safer system.

For applications requiring high energy density, high voltage spinel oxides are promising candidates. In 1997, K. Amine [5] and J. R. Dahn [6] envisioned the '5V' compound of $LiMn_{2-x}M_xO_4$ spinel oxides (M = Ni, Fe with x = 0.5, 1 and M = Ni with $0 < x < 0.5$). For the last several years, intensive efforts have been devoted to the development of $LiNi_{0.5}Mn_{1.5}O_4$

and variants as positive electrode materials for high energy density Li-ion batteries. Subsequent research for the last few years allowed optimizing the electrochemical performance and selecting the $LiNi_{0.4}Mn_{1.6}O_4$ composition (named LNM hereafter) for future developments. This composition shows the highest discharge capacity ($137 mAh \cdot g^{-1}$ for the first cycle) and higher capacity retention than $LiNi_{0.5}Mn_{1.5}O_4$ (about 7% of capacity fading after 100 cycles *vs.* Li^0).[7] The major challenge comes now from the electrolyte/electrode interface, where the discontinuity in charge distribution and extreme discrepancy in electric forces induce diverse processes that eventually determine the kinetics of Li ion intercalation.[8] However, much of these processes and mechanisms still remain poorly understood in particular for high potential materials. For the high voltage spinel compound, the main issue is the side electrolyte oxidation reaction at high voltage yielding too large capacity loss due to self-discharge. Indeed, after two weeks of storage in charged state LNM/LTO cells lose about 30 % of their discharge capacity, and 70-80 % after three months.[9] The result is even worse with graphite negative electrodes (LNM/C cells).[7] Previously, we have investigated the mechanisms occurring at electrode/electrolyte interfaces in LNM/LTO cells, that are responsible for capacity fading and self-discharge processes.[9,10] A passivation film containing organic species coming from decomposition of the solvents at high potential was evidenced at the surface of the LNM electrode after cycling. Interestingly, the surface of the LTO negative electrode was also covered by a thick passivation film, showing transfer of species from the positive to the negative electrode.[9] Interfacial problems at positive electrode have been early identified of importance because they lead to performance degradation of the battery upon aging and cycling.[11] However the chemical, physical and structural properties of the interfacial layer at positive electrode, and their modification upon cycling, are still poorly known, and need further investigation.

Typically, electrolyte additives can affect the reactions of decomposition of the electrolyte and either alter the nature of the decomposition products or lead to the formation of a protective passive layer on the surface of the active material.[12] In this regard, new lithium salts [13] and additives [14,15] for electrolyte, or surface treatments [16] for active material have been studied to promote the formation of a stable passive layer aiming at the improvement of the electrochemical performance. Recently, it was shown that anhydrides (especially succinic anhydride) could have a beneficial effect on the capacity retention of various Li-ion systems, including high-voltage systems.[17,18]

In this paper we studied glutaric anhydride (named GA hereafter) as electrolyte additive in order to improve the performances of the LNM/LTO system. We especially focus on the role of GA on electrode/electrolyte interfacial mechanisms. This study was carried out with the help of three complementary techniques: Nuclear Magnetic Resonance (NMR), X-ray Photoelectron Spectroscopy (XPS) and Electrochemical Impedance spectroscopy (EIS). XPS provides surface chemical characterisation of passivation films (probe depth ~5 nm). NMR is widely used in the field of lithium batteries for structural characterization of active materials,[19,20,21] but thanks to a specific experimental procedure (detailed in the experimental section) it is also possible to separate the signal arising from the passivation layer from the signal of the electrode active material to investigate electrolyte decomposition products.[22,23,24] Finally, EIS provides an electrical characterization and, with the help of equivalent circuit modelling, allow us to access additional information on the interfacial mechanisms.

2. Experimental section

2.1. Materials synthesis:

High voltage nickel manganese spinel oxide $LiNi_{0.4}Mn_{1.6}O_4$ (LNM) was prepared by solid state reaction, starting from stoichiometric proportions of the respective carbonates $MnCO_3$,

Li_2CO_3 and $NiCO_3 \cdot 2Ni(OH)_2$. Pure powders were obtained after mechanical activation using extensive ball-milling in hexane (PM100 Retsch equipment), and successive thermal treatments at high temperatures (10 h at 600°C and 15 h at 900°C) with specific cooling rate, usually 1.0°C.min^{-1}. Particles were then treated in mildly acidic aqueous solution to separate agglomerates and to clean surfaces. The obtained material has a specific surface area of ~0.7 m².g^{-1} and particle sizes between 1 and 20 µm.

Pure spinel oxide $Li_4Ti_5O_{12}$ (LTO) was obtained after multi steps energetic ball-milling of TiO_2 and Li_2CO_3 in stoichiometric proportions in hexane, and thermal treatments at temperatures up to 900°C during several hours, with a final quick treatment under an argon atmosphere, as previously described.[25] The obtained product has a specific area of 13.5 m².g^{-1} and laser granulometry revealed two populations of particles between 0.1 and 100 µm size.

2.2. Electrochemical cycling conditions:

Electrochemical tests were realized in 2032 type coin-cells, using thin composite electrodes prepared by thoroughly mixing active material (spinel oxides) with Super P carbon black (Timcal) and PVdF binder (polyvinylidenedifluoride - Solef 1015, Solvay) in NMP (N-methyl-pyrrolidone). Weight proportions of active material/carbon/binder are 89/6/5 for the LNM electrode and 82/12/6 for the LTO electrode. As-prepared mixtures were coated onto aluminium foils using a doctor blade with 100 µm gap for the positive electrode and 140 µm gap for the negative one. The loading was ~7mg of active material (~0.8 mAh.cm^{-2}). The electrodes were balanced to be limited by the positive electrode active mass (1.54 cm^2 and 2.00 cm^2 discs for positive and negative electrodes in coin cells, respectively). Electrodes were dried for 24 h at 55°C, pressed (6.5 t.cm^{-2}) and finally dried again for 48 h at 80°C under vacuum. Coin cells were assembled in an argon-filled dry box (< 1 ppm O_2/H_2O) with a microporous polypropylene separator (Celgard® 2400). The liquid electrolyte was a mixture of ethylene carbonate, propylene carbonate and dimethylcarbonate (1:1:3 in weight),

containing $LiPF_6$ as salt (1 $mol.L^{-1}$). Two series of cells were studied, without electrolyte additive and with 2% of glutaric anhydride (GA). The GA was purchased from Aldrich (purity 95%) without any additional in-house purification process.

Electrochemical lithium insertion/extraction was monitored with an Arbin automatic cycling data recording system (Arbin, Texas, USA), operating in galvanostatic mode. LNM/LTO cells were tested between 1.5 and 3.5V at ambient temperature at ~C/5 rate (26 $mA.g^{-1}$). In parallel with coin-cells, pouch-cells were built with the same electrode balancing and cycled in the same conditions, which allowed easy observation of gas release during cycling by the swelling of the cell.

For ^{19}F NMR characterization purpose, some LTO electrodes were prepared using carboxymethylcellulose (CMC) as a fluorine free binder. LTO electrodes were processed with Super P carbon (TIMCAL) as the conductive agent and CMC (DS ~ 0.7, Mw ~ 90,000 Aldrich) as binder, according to the electrode formulation: 85 wt.% active material, 10 wt.% Super P carbon and 5 wt.% CMC.

2.3. Characterization techniques :

XPS measurements were carried out with a Kratos Axis Ultra spectrometer, using a focused monochromatized Al Kα radiation (hν = 1486.6 eV). The XPS spectrometer was directly connected through a transfer chamber to an argon dry box, in order to avoid moisture/air exposure of the samples. For the Ag $3d_{5/2}$ line the full width at half maximum (FWHM) was 0.58 eV under the recording conditions. The analyzed area of the samples was 300×700 μm^2. Peaks were recorded with a constant pass energy of 20 eV. The pressure in the analysis chamber was around 5.10^{-9} mbar. Short acquisition time spectra were recorded before and after each normal experiment to check that the samples did not suffer from degradation during the measurements. The binding energy scale was calibrated from the hydrocarbon contamination using the C 1s peak at 285.0 eV. Core peaks were analyzed using

a nonlinear Shirley-type background.[26] The peak positions and areas were optimized by a weighted least-square fitting method using 70 % Gaussian, 30 % Lorentzian lineshapes. Quantification was performed on the basis of Scofield's relative sensitivity factors.[27]

^{7}Li and ^{19}F NMR measurements were carried out at room temperature on a Bruker Avance-500 spectrometer (B0 = 11.8 T, Larmor frequency ν_0 = 194.369 MHz for ^{7}Li resonance and ν_0 = 470.592 MHz for ^{19}F resonance). Single-pulse ^{7}Li MAS spectra were obtained by using a Bruker MAS probe with a cylindrical 2.5 mm o.d. zirconia rotor. Spinning frequencies up to 25 kHz were used. A short single pulse length of 1 µs corresponding to a nonselective π/2 pulse was applied. For ^{7}Li spectra, recycle time was 0.5 s and a spectrometer dead time (preacquisition delay) of 100 µs was used before each acquisition allowing the separation of the surface lithium signal from the bulk signal. ^{19}F NMR spectra were acquired using a Hahn echo sequence to discard the significant contribution from the probe signal and a 5 s recycle time and a 3 ms pulse were used. In the particular case of paramagnetic materials, NMR spectra are dominated by electron-nucleus dipolar interactions several orders of magnitude stronger than nucleus-nucleus dipolar interaction. The electron-nucleus dipolar interaction decreases quickly with the distance (typically as $1/r^3$ where *r* is the distance between the observed Li nucleus and the paramagnetic centre). Therefore, the dipolar interaction will be considerably weaker when the detected Li nucleus and the paramagnetic centre are in two separate phases or even in intimately mixed compounds. The decay of the magnetization corresponding to lithium within the paramagnetic material is therefore considerably faster compared to that of lithium contained with diamagnetic surface species. Using a preacquisition delay longer than the magnetization decay of the "paramagnetic" lithium allows detecting only diamagnetic species on the surface of the paramagnetic active material.[22] The isotropic shifts, reported in ppm, are relative to an external reference made of 1M aqueous solution of LiCl and CCl_3F set at 0 ppm for ^{7}Li and ^{19}F resonances, respectively.

In order to perform a quantitative analysis, the different spectra have been analyzed considering the total integrated intensity of the signal for each sample. Of course, all parameters were kept as constant as possible for each series of NMR measurements: number of scans, probe tuning process, spinning frequency, etc. The spectra displayed in this work were normalized taking into account the number of scans and the mass of sample. NMR spectra fits were performed using DMfit2010.[28]

Electrochemical Impedance Spectrocopy (EIS) measurements were performed in a 3 electrodes cell (a lithium metal wire and a platinum foil were used as reference and counter electrodes, respectively), in the frequency range 2.10^4 to 9.10^{-4} Hz, with a VMP3 (BioLogic) frequency response analyzer. The excitation signal was 10 mV peak to peak. The equilibrium potential was considered to be reached when the drift in open circuit voltage remained less than 0.1 mV for 1 hour. The liquid electrolyte used was the same as for cycling experiments, *i.e.* a mixture of ethylene carbonate, propylene carbonate and dimethylcarbonate (1:1:3 in weight), containing $LiPF_6$ as salt (1 $mol.L^{-1}$), first without and then with 2% GA additive. Fitting of the impedance diagrams was performed with the Zplot® software from Scribner Associate.

3. Results and discussion

3.1. Electrochemical cycling tests:

Figure 1 shows a comparison of the electrochemical behaviours of a LNM/LTO cell cycled between 1.5 and 3.5 V at 20°C and a C/5 rate without (green) and with (blue) 2% of GA additive. Figure 1a shows the charge-discharge voltage profiles for the first cycle. We can observe two plateaus at 3.15 and 3.2 V associated to Ni^{2+}/Ni^{3+} and Ni^{3+}/Ni^{4+} oxidation potentials (4.7 and 4.75 V *vs.* Li^+/Li, respectively) and a short "plateau" at 2.4 V associated to Mn^{3+}/Mn^{4+} (~4 V *vs.* Li^+/Li). Without GA additive, the reversible capacity at the first cycle is

133 mAh.g^{-1}, with a small irreversible capacity loss lower than 10 mAh.g^{-1}. With 2% of additive the reversible capacity is about the same (130 mAh.g^{-1}) with an irreversible capacity loss of 14 mAh.g^{-1}.

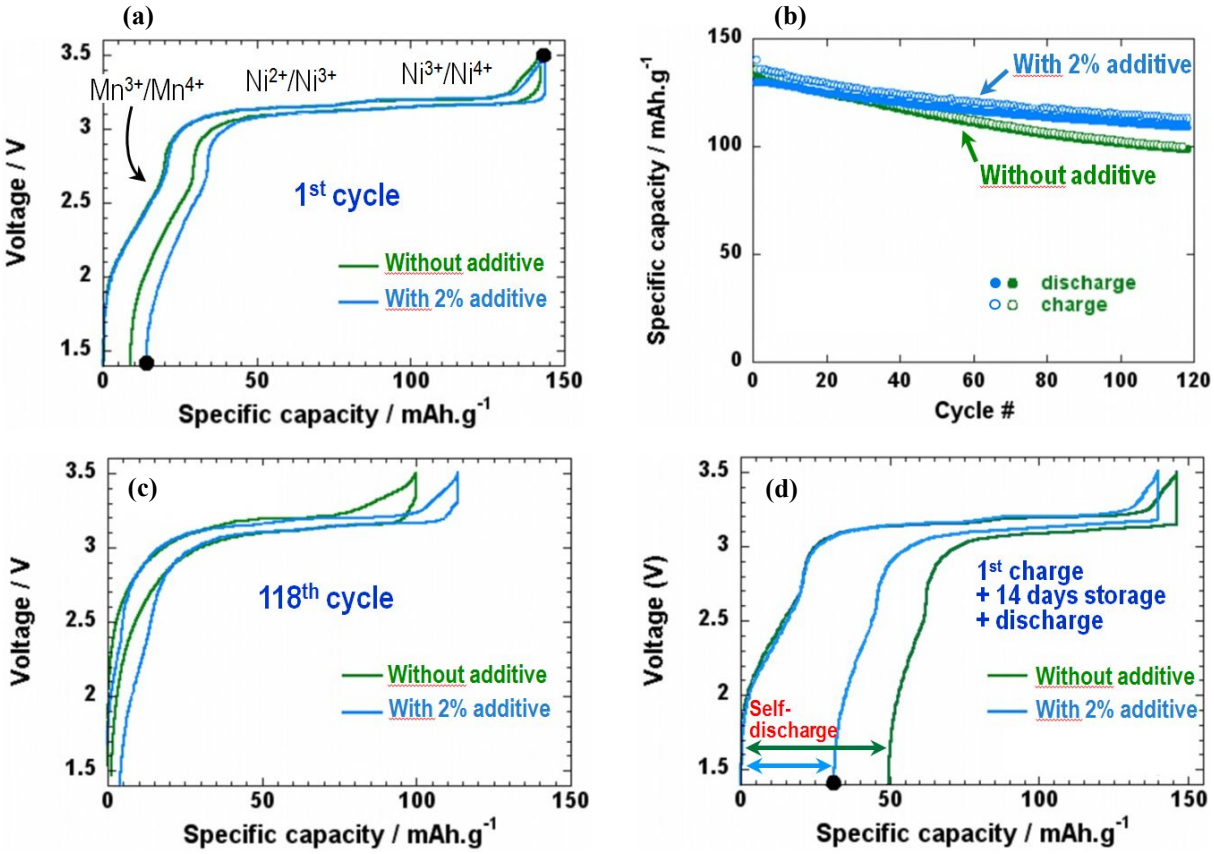

Figure 1: Comparison of electrochemical behaviours of a LNM/LTO coin cell cycled between 1.5 and 3.5 V at 20°C and a C/5 rate with and without GA as electrolyte additive. **(a,c)** Charge-discharge voltage profiles of the 1st and 118th cycles. **(b)** Capacity retention *vs.* cycle number, **(d)** Charge-discharge voltage profile obtained by a 1st charge followed by 14 days of storage in charged state (open-circuit voltage) and a discharge.

Figure 1b shows the capacity retention upon cycling. After ~120 cycles without additive the discharge capacity is 100 mAh.g^{-1} corresponding to a 25% capacity loss with respect to the first cycle. With 2% of additive the capacity retention is much better since the reversible capacity is 110 mAh.g^{-1} which corresponds to a capacity loss of about 15%.

Figure 1c shows the 118th cycle. It is clear that without additive the Mn^{3+}/Mn^{4+} "plateau" at 2.4 V has totally disappeared, whereas with 2% of additive it is partially retained, resulting in the better observed capacity retention. This point will be discussed below.

The most significant effect of GA addition is the hindering of the self-discharge process, as shown in Figure 1d. In this case the charge-discharge voltage profile is obtained after a first charge, followed by 14 days of storage in charged state (open-circuit voltage) and a final discharge. The reversible capacity is only 96 $mAh.g^{-1}$ without additive, which corresponds to a significant 28 % capacity loss with respect to a normal first cycle (without storage in charged state). With 2% of additive the capacity retention is 109 $mAh.g^{-1}$, which corresponds to an improved 16 % only capacity loss. As a summary, the electrochemical performance of the system without additive are rather poor and the presence of GA allows improving significantly (but not sufficiently) the electrochemical behaviour of LNM/LTO cells.

Figure 2: Photograph of a LNM/LTO pouch cell after 118 cycles between 1.5 and 3.5 V at 20°C and a C/5 rate with 2% of GA additive.

In parallel with coin-cells, pouch-cells were cycled in the same conditions, which allowed easy observation of gas release during cycling by the swelling of the cell. Figure 2 shows a photograph of a pouch cell after 118 cycles using 2% of GA as additive. An important swelling of pouch cells is observed after long cycling (no differences were observed with and

without additive). Therefore, the electrochemical behaviour improvement induced by GA is not linked to a decrease of the gas release within the cell. The purpose of the following discussion is to understand the mechanisms of action of this additive by investigation of the surface of the electrodes after the electrochemical tests. We present now our combined XPS / NMR / EIS investigation.

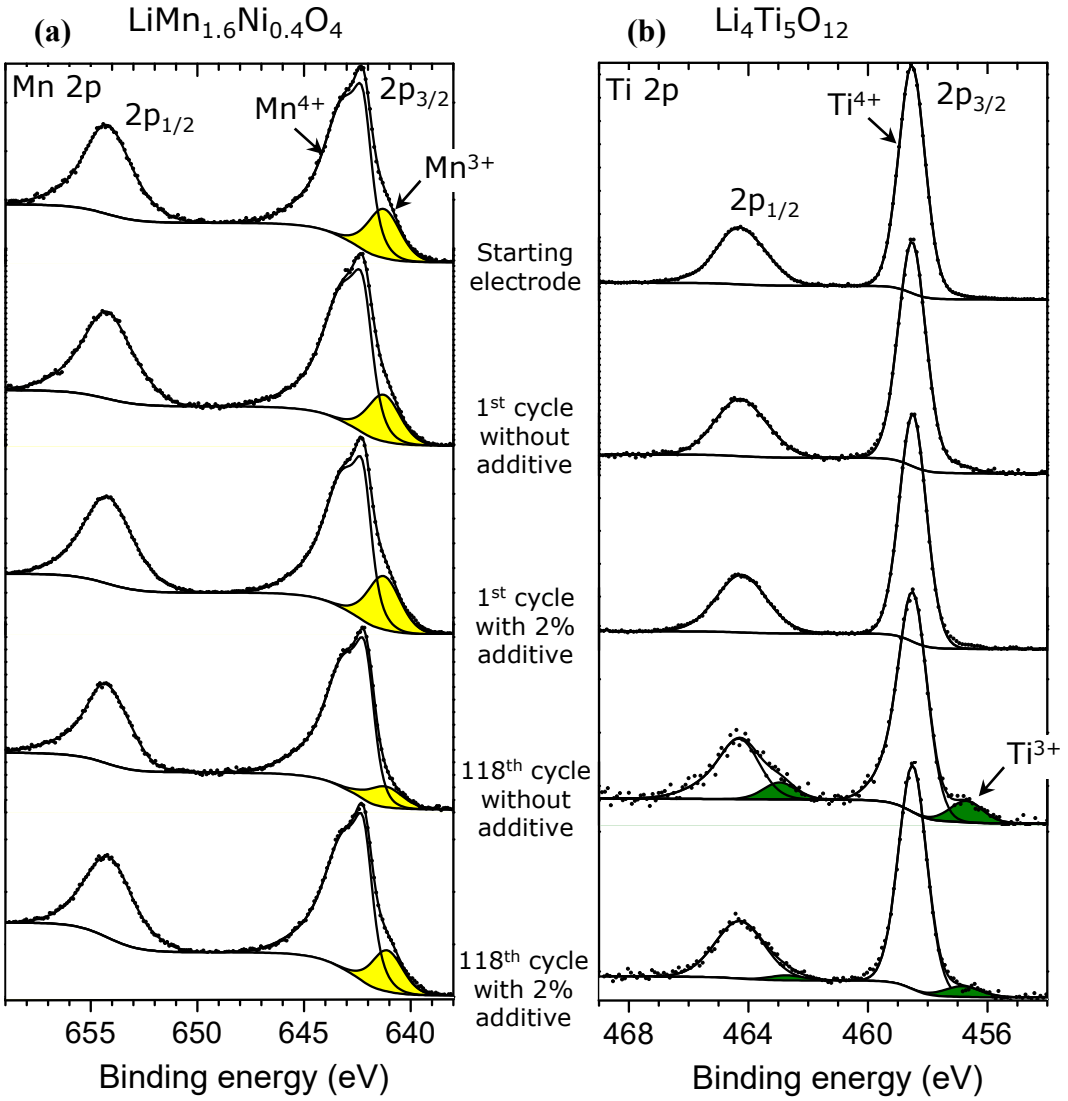

Figure 3: **(a)** Mn 2p XPS spectra of the LNM positive electrode and **(b)** Ti 2p XPS spectra of the LTO negative electrode: starting electrode, 1st cycle without and with 2% of additive, 118th cycle without and with 2% of GA additive.

3.2. LNM and LTO active materials surface during cycling :

It is to be noted that X-ray diffraction (XRD) measurements were carried out on cycled electrodes, and that no structural differences could be evidenced after long cycling. XRD patterns of the LNM electrode (pristine powder and composite electrode after 118 cycles) are available as Supporting Information (Figure S1). There is no detectable structural degradation of the bulk active materials upon cycling.

Concerning the surface of the active materials, Figure 3a and 3b show Mn 2p and Ti 2p XPS spectra of the LNM and LTO electrodes, respectively, for the following samples: starting electrode, first cycle without and with 2% of additive, 118^{th} cycle without and with 2% of additive. Due to spin-orbit coupling each Metal 2p spectrum is split in two parts ($2p_{3/2}$ and $2p_{1/2}$), with an area ratio of about 2/1.

The Mn 2p spectrum of the starting LNM electrode shows a complex shape. The Mn $2p_{3/2}$ component consists in a maximum (with a fine structure) at 642.3 eV assigned to Mn^{4+} ions with a shoulder at 641.2 eV assigned to Mn^{3+} ions, in good agreement with the theoretical formula of the compound $Li^{+}Mn^{4+}_{1.4}Mn^{3+}_{0.2}Ni^{2+}_{0.4}O_4$. The fine structure of the Mn^{4+} peak (642.3 and 643.1 eV) does not result from the presence of two different oxidation states of manganese, but from final state effects due to the XPS photoemission process (multiplet splitting effects, or local *vs.* non-local screening effects [29,30]). In the Mn $2p_{1/2}$ component the resolution is too low to evidence this Mn^{4+} fine structure and the Mn^{3+} shoulder. Therefore it is not represented in the figure.

After the first cycle, either without or with 2% of additive the Mn 2p spectra are very similar to that of the starting electrode, in good agreement with the reversibility of the electron transfer over the first cycle. After 118 cycles, however, some differences can be noticed. The intensity of the Mn^{3+} component at 641.2 eV has almost disappeared when no additive is used, showing that the LNM material is not perfectly discharged. This is not true

with 2% of additive. This observation is consistent with the disappearance of the Mn^{3+} oxidation step at 2.0-2.5 V in the charge-discharge voltage profile of the 118th cycle without additive in figure 1c, and its better retention with 2% of additive, as discussed above.

The Ti 2p spectrum of the starting LTO electrode is simpler. A unique peak corresponding to Ti^{4+} ions is observed either for the $2p_{3/2}$ or the $2p_{1/2}$ component (458.6 and 464.4 eV, respectively). After the first cycle no difference is observed, either without or with 2% of additive. However after 118 cycles a Ti^{3+} component ($2p_{3/2}$ at 456.8 eV) is observed, which shows that the $Li_4Ti_5O_{12}$ material is still partially charged. The intensity of this component is lower when 2% of additive is used in the electrolyte. This observation is in good agreement with the irreversible process concerning the valence state of manganese observed at the positive electrode, and shows that this irreversible process concerns both electrodes upon electrochemical cycling. This result also proves that the use of GA is efficient to reduce this phenomenon that contributes to the capacity loss upon cycling. The analysis of electrode/electrolyte interfaces will provide more information about the involved mechanisms.

3.3. LNM electrode/electrolyte interface:

3.3.1. ^{7}Li NMR:

^{7}Li NMR has been performed to investigate the lithiated species that were deposited in the passivation film at the surface of the LNM electrodes. To this aim, a specific procedure allowing separation of the surface lithium signal from the bulk signal was used (see experimental section).

Figure 4a and 4b show the ^{7}Li NMR spectra without and with 2% of additive, respectively, for the following samples: first charge, first cycle, first charge followed by 14 days of storage in charged state (open-circuit voltage) and a final discharge, 30th and 118th cycles. Two types of lithium signals are detected.

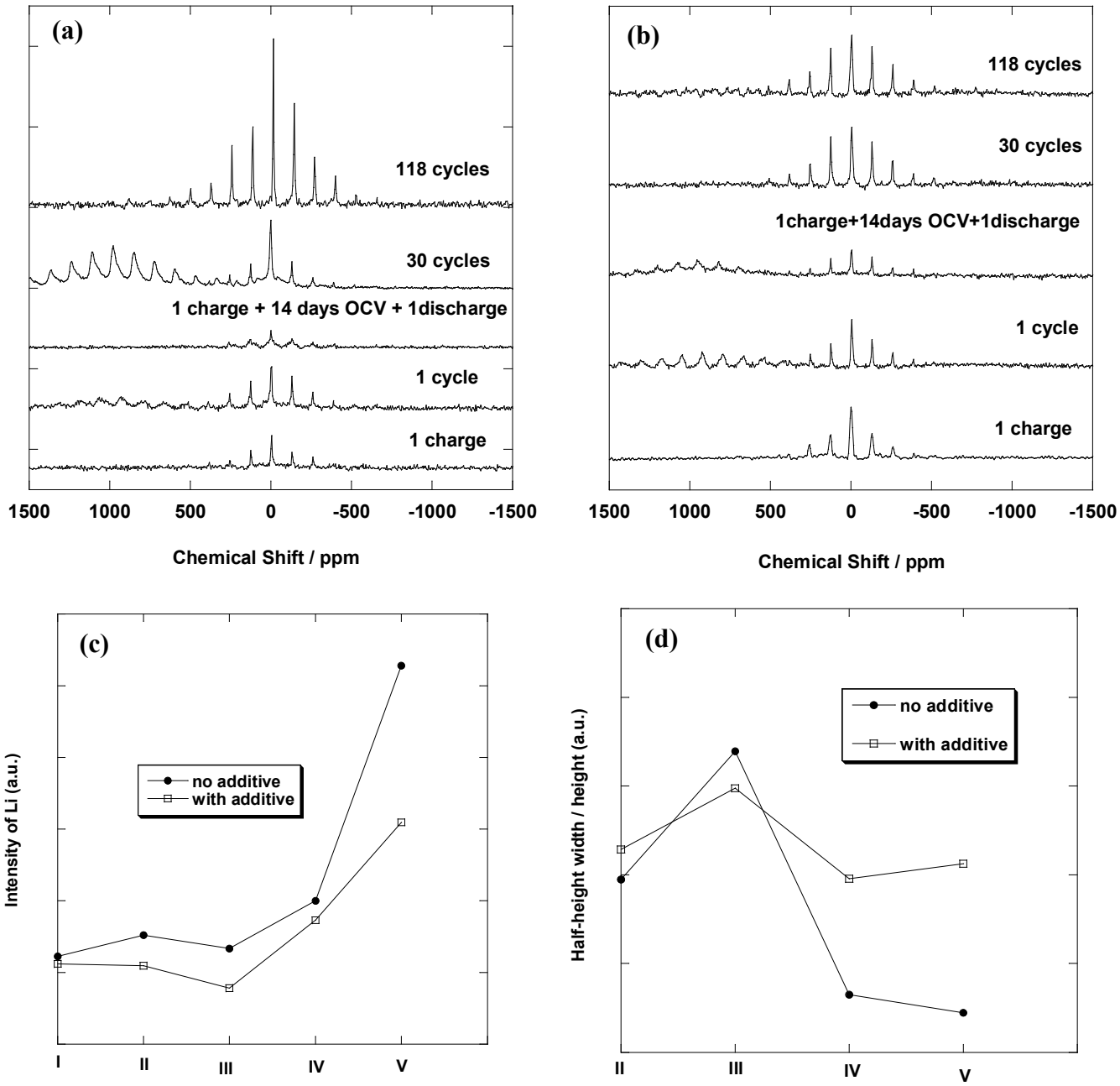

Figure 4: Normalized ^{7}Li MAS NMR spectra of the LNM positive electrode: **(a)** without additive and **(b)** with 2% of GA. **(c)** Evolution of the normalized integrated intensities of ^{7}Li MAS NMR spectra. **(d)** FWHM of ^{7}Li NMR spectra normalized to the height.
I, the first charge; **II**, the first cycle; **III**, the first discharge after a 14-days rest at 3.5V; **IV**, after 30 cycles; **V**, after 118 cycles.

The narrow signal at 0 ppm is assigned to diamagnetic species deposited at the electrode/electrolyte while the signal arising at 800-1100 ppm seems to be due to lithium in the bulk of the active material based on the significant typical Fermi-contact shift. This second signal is not always detected and seems to appear quite randomly. Considering its intensity compared to the surface signal, it most probably concerns only a very small volume of the electrode and must be seen as a residual signal that was not eliminated by the use of a long pre-acquisition delay. No straightforward relation could be found between the detection of that (random) signal and the state of charge or number of cycle of the electrode. We tentatively ascribe the detection of this residual signal to a slightly different modification of the surface structure of the active material after the contact with the electrolyte. It supposes obviously a reaction between the electrode material and the electrolyte.

The following discussion will be focused on the surface lithium signal at 0 ppm since the evolution of the surface species is the target of the present investigation. A relatively low intensity of surface lithium is found for the samples that underwent a long rest (14 days) at high potential (3.5V *vs.* LTO, *i.e.* 5 V *vs.* Li^+/Li) after the first charge, especially when compared with the spectra of samples corresponding to a simple cycling condition (no rest at the end of charge). The same phenomenon is observed whether additive is used or not, suggesting a partial decomposition or dissolution of the diamagnetic lithiated species that were deposited on the surface of the electrode material upon the first charge for a long exposure at high potential. This phenomenon is nevertheless less visible when 2% of additive is used, suggesting a lesser extent of Li-containing species decomposition/dissolution for a long exposure at high potential.

In both cases the same general trend is observed upon cycling: the intensity of surface Li signal is increasing with the cycling number, especially for electrodes after 118 cycles in electrolyte without additive. The integrated intensities of surface Li signals of the two

different electrodes were quantified by fitting the spectra using the software DMfit2010 [28] and the deduced values are shown in Figure 4c.

Except for the first charge, for which intensities are quite similar, the ^{7}Li integrated intensity is always lower when additive is used and the difference between the two types of electrodes becomes significant after 118 cycles. This result suggests that GA additive restrains the decomposition of the electrolyte lithium salt and the deposition of lithiated species such as LiF on the surface of the active material although the phenomenon is not completely suppressed.

The analysis of the profile of the sidebands manifold can also bring useful information when examined in the light of the evolution of the amount of lithiated species observed. In previous works,[16] it has been shown that the spectrum or sidebands manifold width can be linked to the strength of the nucleus-electron dipolar interaction between lithium in the interphase and paramagnetic electrode material. This interaction is then linked to the intimacy between the diamagnetic surface species and the bulk of paramagnetic electrode material. More details can be found in ref. [11,14]. In brief, a broad sidebands manifold will indicate a strong interaction between Li nuclei in the interphase and transition metals in the active material and an overall short distance between them. A narrow sidebands manifold will indicate an overall or average longer distance between the surface Li and the transition metals, implying an overall weaker intimacy between the lithiated species in the passivation film and the surface of active material. In the figure 4d is reported the evolution of full width at half-height (FWHM) of sidebands manifold of ^{7}Li MAS-NMR spectra for the studied samples.

Considering first the evolution for samples analyzed after 1, 30 and 118 cycles, in the absence of additive, the clear overall decrease of the FWHM indicates that the sidebands manifolds become thinner for longer contact times and thus more relative intensity is found in the central part of the spectrum as the electrochemical cycling goes on. It shows that

additional lithiated species with a weaker interaction with the paramagnetic bulk of active material are progressively included in the surface deposits. These results indicate that the ^{7}Li NMR integrated intensity growth observed for the same samples does not seem to correspond to the further covering of the surface of active material by lithiated products coming from the decomposition of the electrolyte but can be attributed mostly to the stacking of lithium containing species on the top of the initial deposits, farther from the paramagnetic bulk. On the other side, the values of the FWHM for electrode cycled in the presence of additive are clearly more stable. This result, combined with the slow increase of integrated intensity suggests a further covering of the surface of the active material by lithiated species or a better distribution of the lithiated species on the surface of active material rather than a stacking of species leading to thick discrete deposits. Thus, when GA is used, a rather stable and homogenous surface film seems to form and no significant change in the interaction between the active material and this film is detected upon cycling.

In the particular case of electrodes recovered after one charge (*i.e.* in the oxidized state), the values of the FWHM are not discussed here, due to the different oxidation states of transition metals. As a matter of fact, the number of unpaired electrons localized on transition metal ions is different: Ni^{2+} (t_{2g}^{6} e_g^{2}), Mn^{3+} (t_{2g}^{3} e_g^{1}), and Mn^{4+} (t_{2g}^{3} e_g^{0}) in discharged and Ni^{4+} (t_{2g}^{4} e_g^{2}) and Mn^{4+} (t_{2g}^{3} e_g^{0}) in charged state, respectively. The change in the number of unpaired electrons is expected to alter the magnitude of the electron-nucleus dipolar interaction and thus, the width of the sidebands manifold. Therefore, the width of sidebands manifold for samples in the charged and discharged states cannot be directly compared. Further studies are necessary to understand the influence of the change of oxidation state within the electrode material on the shape of the ^{7}Li NMR spectra of surface diamagnetic species.

3.3.2. XPS:

Quantitative data from XPS spectra of the pristine LNM electrode, and after 118 cycles with and without additive are given in Table 1.

Table 1: XPS binding energies (B.E., eV) and atomic percentages (at. %) of elements measured at the surface of LNM positive electrode: starting electrode, and after 118 cycles without and with 2% of additive.
* CH_2 component of PVdF was fixed to be equal to CF_2

Peak	B.E. (eV)	Starting electrode at. %	118 cycles without additive at. %	118 cycles with 2% additive at. %	Attribution
O 1s	529.9	14.0	8.4	2.0	LNM
	531-534	5.7	15.1	23.2	Surface species
Mn $2p_{3/2}$	642.3	6.6	4.4	1.1	LNM
Ni 3p	67.3	1.6	1.0	0.3	LNM
Li 1s	54.1	6.0	3.1	1.0	LNM
	55.9	---	1.2	0.4	LiF + other lithiated species
C 1s	284.5	25.8	15.6	3.5	Conductive carbon
	286.5	9.8	6.4*	6.5*	PVdF (CH_2)
	290.9	9.3	6.4	6.5	PVdF (CF_2)
	285-290	2.9	21.8	40	Surface species
F 1s	685.0	---	0.9	0.3	LiF
	687.9	18.3	14.4	14.7	PVdF (+ $Li_xPO_yF_z$)
P $2p_{3/2}$	134.1	---	0.9	0.1	phosphates
	135.7	---	0.4	0.5	$Li_xPO_yF_z$

Especially, the Mn/Ni ratio at the pristine LNM electrode surface is 4.1. For the electrode after 118 cycles it is 4.4 without additive and 3.7 with the additive. Since the theoretical Mn/Ni ratio is 4.0 in the bulk, these data show that the Mn/Ni ratio remains close to the expected value at the surface of the LNM electrodes. Therefore, despite a slight dissolution

process that can be evidenced by the presence of 0.6-0.9 % of Mn at the LTO electrode surface after 118 cycles (see Table 2), this dissolution process does not lead to a significant change of the surface composition of LNM electrodes.

Table 2: XPS binding energies (B.E., eV) and atomic percentages (at. %) of elements measured at the surface of LTO negative electrode: starting electrode, and after 118 cycles without and with 2% of additive.
* CH_2 component of PVdF was fixed to be equal to CF_2

Peak	B.E. (eV)	Starting electrode at. %	118 cycles without additive at. %	118 cycles with 2% additive at. %	Attribution
O 1s	529.9	11.2	3.1	1.6	LTO
	531-534	4.1	18.7	20.7	Surface species
Ti $2p_{3/2}$	458.6	5.0	1.6	0.7	LTO
Li 1s	54.6	5.0	1.2	0.7	LTO
	55.7	---	6.8	5.4	LiF + other lithiated species
C 1s	284.2	28.6	7.1	5.0	Conductive carbon
	286.5	9.7	4.4*	3.8*	PVdF (CH_2)
	290.9	9.7	4.4	3.8	PVdF (CF_2)
	285-290	9.9	33.9	43.4	Surface species
F 1s	685.0	---	6.5	2.7	LiF
	687.9	16.8	9.6	10.2	PVdF (+ $LiPF_6$ + $Li_xPO_yF_z$)
P $2p_{3/2}$	134.1	---	2.1	0.6	phosphates
	135.6	---	---	0.2	$Li_xPO_yF_z$
	136.9	---	---	0.3	$LiPF_6$
Mn $2p_{3/2}$	641.4	---	0.6	0.9	dissolved Mn

The deposition of carbon- and oxygen-containing species at the LNM electrode/electrolyte interface was followed by C 1s and O 1s XPS spectra. Figure 5 shows O 1s spectra of the LNM positive electrode (a) without additive, (b) with 2% of additive, respectively, for the

following samples: starting electrode, after the first, 30th and 118th cycles, and after 14 days of storage in charged state before discharge.

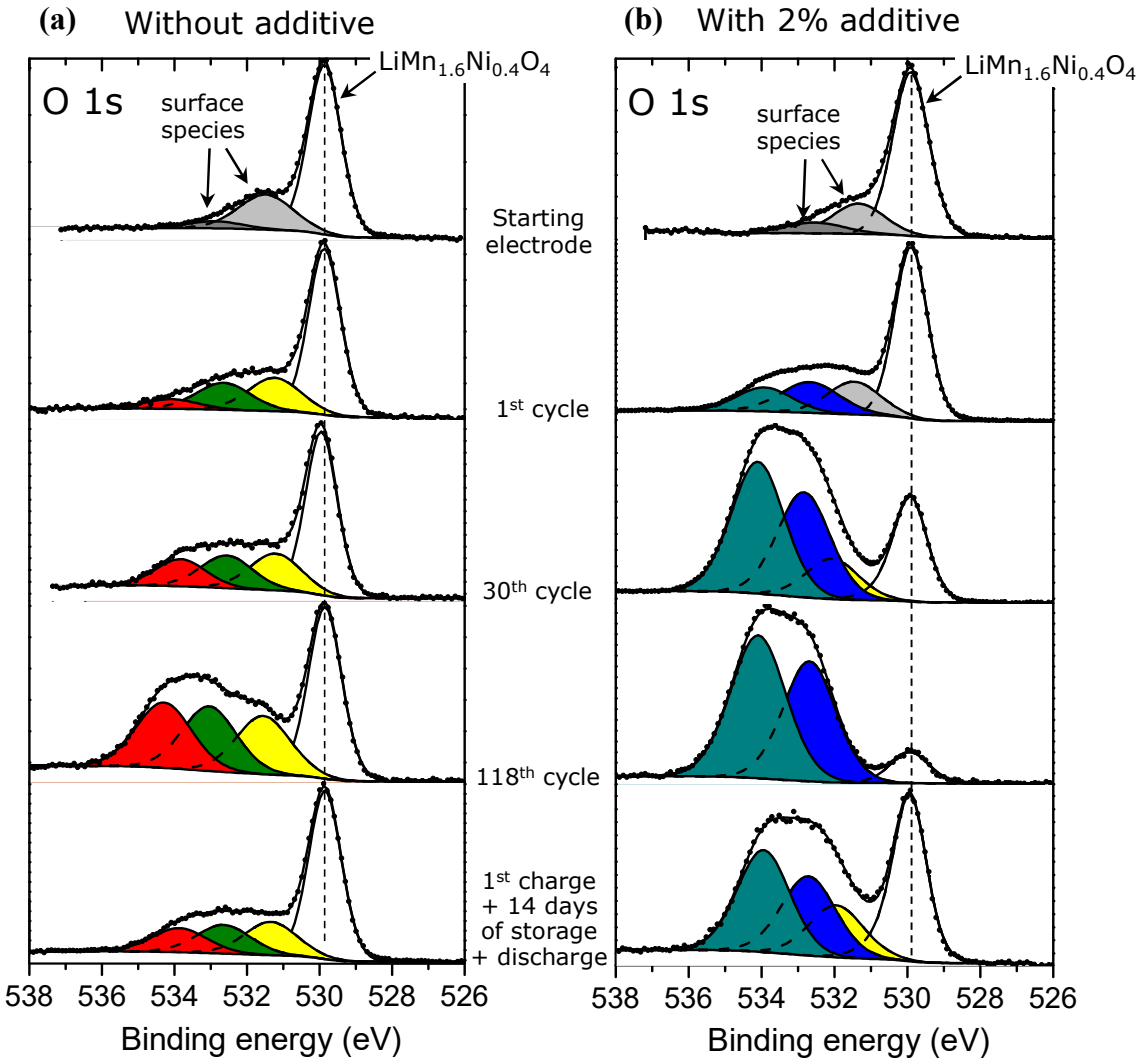

Figure 5: O 1s spectra of the LNM positive electrode **(a)** without additive, **(b)** with 2% of GA: starting electrode, 1st, 30th and 118th cycles, and after 14 days of storage in charged state before discharge.

The spectrum of the starting LNM electrode displays a narrow peak at 529.9 eV which is characteristic of O^{2-} anions of the crystalline network. The second peak at higher binding energy (531.5 eV) is assigned to weakly adsorbed species at the surface, and also probably to

oxygen anions of the subsurface, which have a deficient coordination.[31] The very weak component at ~533 eV may be also assigned to weakly adsorbed species.

Upon cycling, when no additive is used in the electrolyte (figure 5a) the O 1s spectrum shows an increase of three components at 531.5, 533 and 534.4 eV, which can be attributed to the deposition of new oxygenated species at the surface of the electrode. These species result from the oxidation of the electrolyte at the positive electrode surface, especially the solvents, due to the very high potential reached by this electrode upon charge (up to 5 V *vs.* Li^+/Li). The gradual increase of these components with respect to the signature of the active material shows the gradual increase of the thickness and/or covering percentage of the passivation layer formed at the surface of the electrode.

After 118 cycles, the amount of surface oxygenated species is 15%, about twice as large as the amount of oxygen of the LNM electrode material in the 5 nm thick layer analysed by XPS (see Table 1). Due to the small amount of inorganic species containing oxygen, mainly phosphates and fluorophosphates which can be detected in P 2p spectra (not shown here, see Table 1) the main part of this surface oxygen is attributed to organic species coming from degradation of the solvents.

The O 1s spectrum obtained after 14 days of storage in charged state is very similar to that obtained after 30 cycles, which is in good agreement with an oxidation process of the electrolyte at high potential. Indeed, the time spent by the positive electrode at a voltage higher than 4.5 V *vs.* Li^+/Li is about the same for both experiments (14 and 10 days, respectively).

As shown in figure 5b, when 2% of GA is introduced in the electrolyte the deposition process of new oxygenated species at the surface of the electrode is much more significant. Indeed, two new components are observed at 532.7 and 534 eV. Their intensity is weak after the first cycle. However after 30 cycles, and especially after 118 cycles the covering process

of the electrode by these new oxygenated species is very important, so that the signature of the electrode material appears very weak in comparison. Note that in this case the O 1s spectrum obtained after 14 days of storage in charged state corresponds to a slightly lower amount of deposited species than after 30 cycles. The binding energies observed with 2% of additive are different from the case without additive. Therefore these new components can be attributed to oxygenated species resulting mainly from the degradation of the GA additive at the surface of the electrode. After 118 cycles the amount of additional oxygen accounts for 23% of the composition of the surface.

Figure 6 shows the O 1s and C 1s spectra of pure GA powder as reference sample (the spectra were recorded at -140°C to avoid sublimation of the powder in ultra-high vacuum). The O 1s spectrum consists of two peaks at 532.5 and 533.7 eV with an intensity ratio of about 2/1, which are assigned to terminal and bridging oxygen atoms in the molecule, respectively. The C 1s spectrum consists of three peaks at 285.0, 285.4 and 289.4 eV assigned to the three kinds of carbon environments.

It is interesting to notice that the O 1s signature of the pure GA is different from that of the species deposited at the surface of the electrode when this additive is used in the electrolyte, as previously shown in Figure 5b. Indeed, the main signature of the deposited species consists of two peaks at 532.6 and 534 eV, with very close binding energies with respect to the pure GA, but with a very different intensity ratio. This O 1s signature is thus mainly due to organic compounds resulting from degradation of GA at the surface of the electrode, rather than the anhydride itself. The observed change of intensity ratio between both O 1s components can be attributed to a change of the ratio between terminal and bridging oxygen atoms. A ring opening mechanism of the GA molecule can be therefore expected.

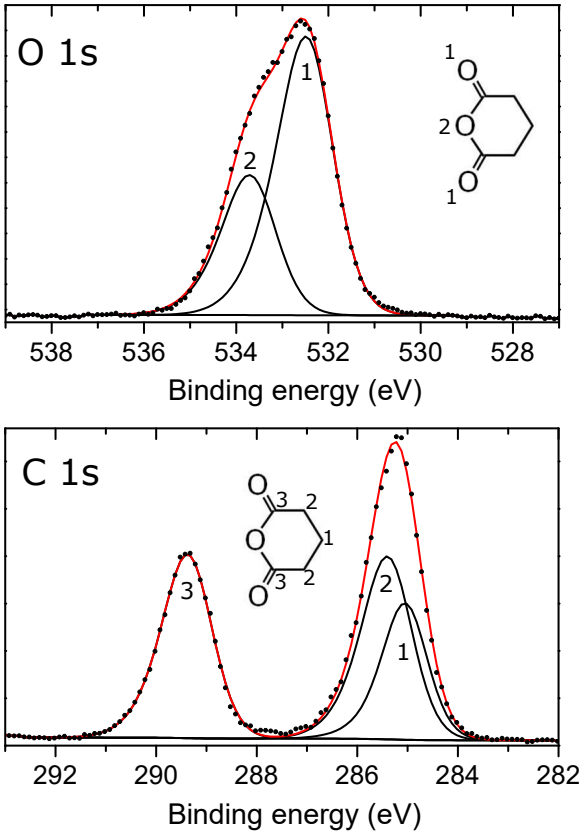

Figure 6: O 1s and C 1s spectra of pure glutaric anhydride (GA).

In order to get more information about the nature of the organic species formed at the surface of the electrode, we analysed the C 1s XPS spectra of the same samples. Figure 7 shows the C 1s spectra of the starting LNM positive electrode and after 118 cycles without and with 2% of additive. The C 1s spectrum of the starting electrode consists of three peaks. The first one at 284.5 eV is due to conductive carbon (carbon black and carbon fibers) and the two other ones at 286.4 and 290.9 eV are assigned to CH_2- and CF_2 environments of carbon in PVdF, respectively. Note that the cumulated C 1s signals of conductive carbon and of PVdF account for 45% of the global XPS signal (see Table 1). Therefore, differences in the C 1s spectra after cycling can be observed only if a very important amount of carbonaceous species is deposited at the surface of the electrode. This could be observed after 118 cycles.

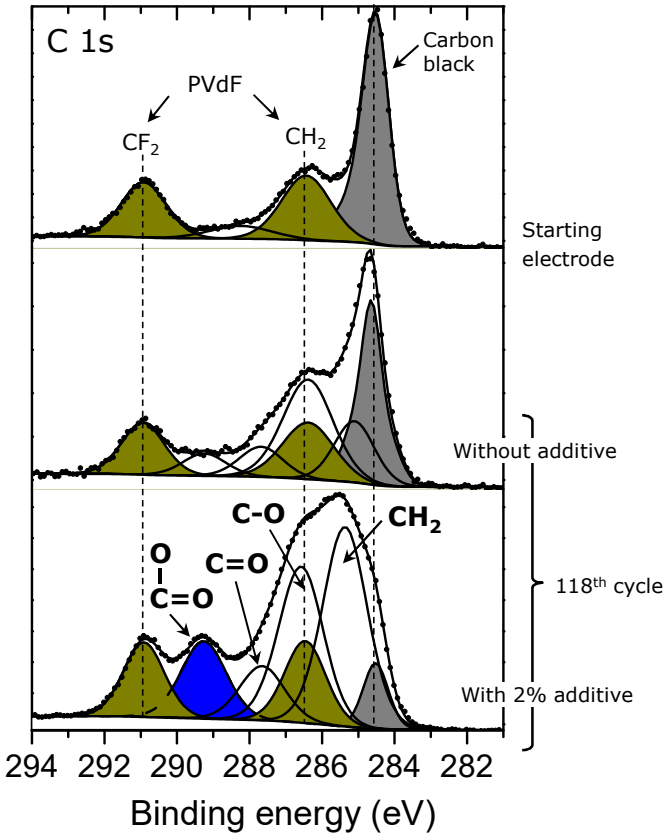

Figure 7: C 1s spectra of the LNM positive electrode: starting electrode and after 118 cycles without and with 2% of GA additive.

After 118 cycles without the additive, we observed a small increase of components at 285, 286.7, 287.9 and 289.3 eV corresponding to -CH_2, C–O, C=O and O=C–O environments of carbon, showing deposition of new species. With 2% of GA additive the intensities of the new peaks were much greater, showing the larger amount of deposited organic species. The characteristic O=C–O environment of the additive was still observed, which means that O=C-O organic functions are still present in the degradation species. The intensity of the characteristic component of conductive carbon decreased significantly (3.5%, see Table 1), which shows it was covered by these new carbonaceous species. On the contrary the characteristic component of PVdF at 290.9 eV was retained, showing that the covering

process concerns preferably the conducting part of the electrode, in good agreement with an electrochemically driven degradation process of the additive at the surface of the electrode. As a summary, the chemical composition of the passivation layer formed by degradation of the additive shown in Table 1 displays its main organic character. The amount of inorganic species (LiF, phosphates, fluorophosphates) is rather low, but the amount of additional carbon and oxygen accounts for more than 60 % of the 5 nm thick layer analysed by XPS. The use of the additive in the electrolyte tends to decrease the proportion of inorganic species in the passivation layer, in good agreement with NMR data shown above.

3.3.3. EIS:

The LNM electrode/electrolyte interface was also checked by EIS. Figures 8a, 8b and 8c show the results obtained without additive and Figures 8d and 8e show those obtained with 2% of GA. The corresponding values of global resistance Z', of film resistance R_f and of charge transfer resistance R_{ct} are given in Table 3. As previously reported without any electrolyte additive,[9] at the positive electrode we can first evidence an electro-adsorption mechanism (adsorption of species which process is mainly governed by the voltage of the electrode, see Supporting Information for details) at the beginning of the cycling tests (experimentally observed on the 1st cycle in Figure 8a and modeled by an equivalent circuit in Figure 9a). Then a passivation phenomenon (covering of the surface of the electrode) takes place upon cycling (experimentally observed at the 30th cycle in Figure 8b and modeled in Figure 9b).

We have also reported that the way the electrode is maintained at its highest voltage (*i.e.* 5V vs. Li) plays a crucial role in the impedance response since continuously maintaining the electrode at a high voltage (experimentally, for sample after 14 days of storage, Figure 8c) makes the passivation film denser, thus resulting in the significant increase of the positive electrode/electrolyte impedance (2 500 Ω.cm^2).

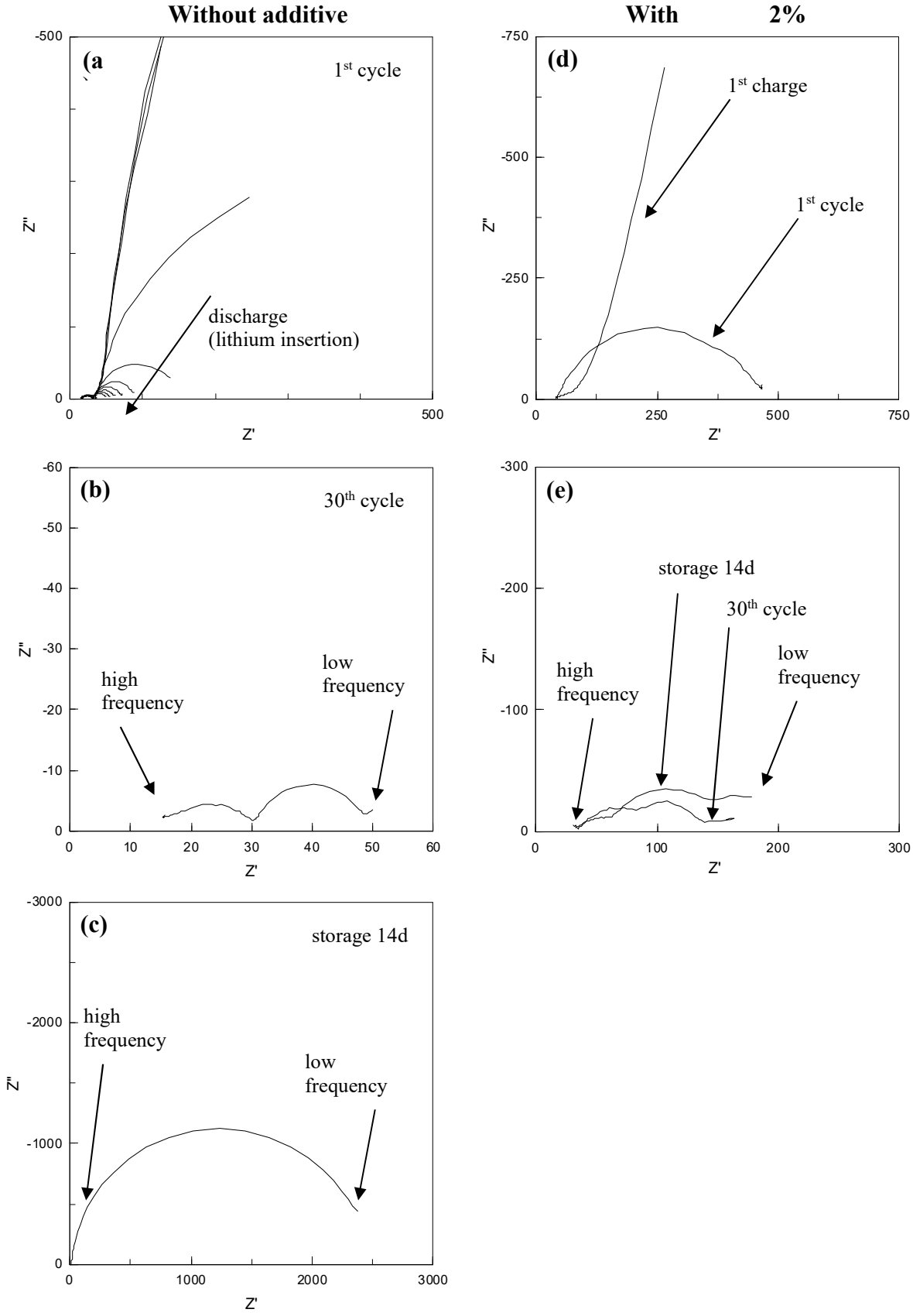

Figure 8: EIS diagrams of the LNM positive electrode: **(a)** evolution during lithium insertion (cell discharge after a first charge, without additive), **(b)** after 30 cycles (without additive), **(c)** after 14 days of storage in charged state before discharge (without additive), **(d)** after the first charge and the first discharge (1st cycle) with 2% of GA, and **(e)** after 30 cycles and after 14 days of storage (with 2% of GA).

In contrast to this, after 118 charge-discharge cycles (*i.e.* after same time spent at the highest voltage), the impedance is lower, suggesting that a less resistive film is formed on the surface of the electrode (more porous film or, in any case, less dense than after storage, due to successive deposition steps), which is consistent with the fact that the electrode voltage reaches here its highest value only intermittently.

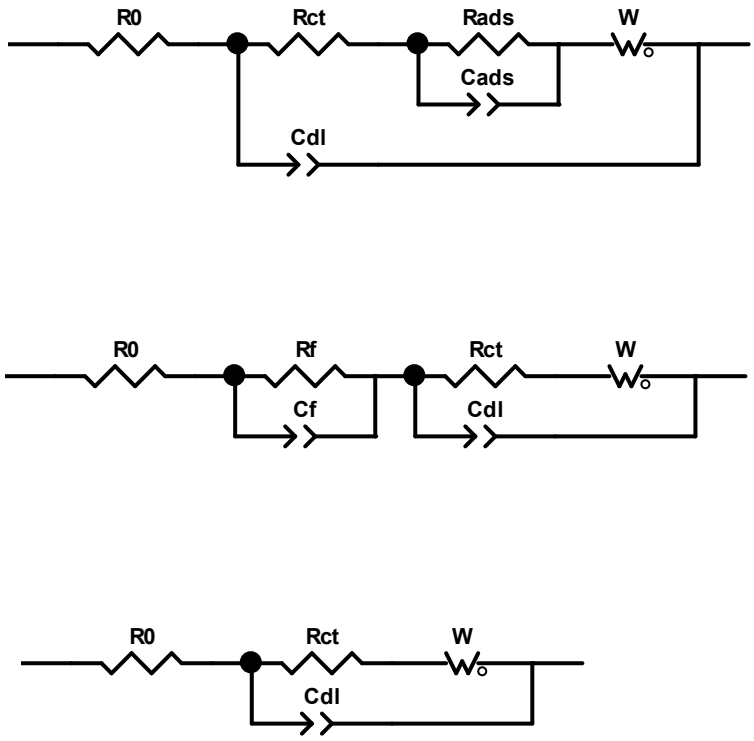

Figure 9: Electrical equivalent circuits: **(a)** electro-adsorption process, **(b)** passivation film process, and **(c)** insertion process (Randles type).

These EIS observations are in good agreement with those obtained by NMR and XPS and together demonstrate that the electrolyte degrades at high voltage (5V vs. Li) and gradually covers the electrode with organic/inorganic species, inducing a progressive increase of the interface impedance (formation of a resistive film). Moreover, the way the positive electrode passes through the highest voltage (continuously or intermittently) plays a key role on the

morphology of the passivation film (dense or porous) and, ultimately, on the global system impedance (large or small).

When adding 2% GA in the electrolyte, we can still evidence, at the positive electrode, as in standard electrolyte, the first mechanism of electro-adsorption at the very beginning of the cycling tests (experimentally observed on the 1st cycle in Figure 8d and modeled by an equivalent circuit in Figure 9a, see Supporting Information for details), but it seems now constrained since, in that case, adsorption does not lead to the same covering rates.

Consider the electrokinetics equations for such a mechanism :

$$\underset{C_{el}}{\left[Li^+\right]_{org}} + \underset{\Gamma(1-\theta)}{surface} \overset{k}{\longleftrightarrow} \underset{\Gamma\theta}{(\left[Li^+\right]_{org}, surface)} \qquad (1)$$

$$\underset{\Gamma\theta}{(\left[Li^+\right]_{org}, surface)} + e^- \underset{k_a}{\overset{k_c}{\longleftrightarrow}} \underset{C_0}{(Li^+, e^-)_{oxide}} + \underset{\Gamma(1-\theta)}{surface} \qquad (2)$$

$$\underset{C_0}{(Li^+, e^-)_{oxide}} \xrightarrow{D_{Li}} \underset{C}{(Li^+, e^-)_{oxide}} \qquad (3)$$

where C_{el}, C_0 and C are the concentration of solvated lithium ions in the electrolyte solution, the concentration of lithium ions in the positive electrode near the interface electrode/electrolyte and the concentration of lithium ions in the positive electrode at equilibrium respectively; Γ is the surfacic concentration of host sites, on the electrode, for adsorbates; θ is the rate of occupied sites.

In that case, an estimate of the surface coverage, θ, at the end of the 1st discharge, gives a value of only 45% compared to the value obtained in standard electrolyte. This means that the surface is already covered by species from the electrolyte (step 1 becomes limited), which is consistent with the large amount of new oxygenated species, evidenced by XPS, at that stage.

Table 3: LNM positive electrode. Resistance values ($\Omega.cm^2$) obtained from the EIS diagrams presented in Figure 8 with and without additive: global resistance Z', film resistance R_f and charge transfer resistance R_{ct}.

LNM electrode	Without additive			With 2% additive		
	30 cycles	118 cycles	Storage 14 days	30 cycles	118 cycles	Storage 14 days
Global resistance Z' ($\Omega.cm^2$)	50	350	2 500	150	200	180
Film resistance R_f ($\Omega.cm^2$)	20	180	1 200	15	25	30
Charge transfer resistance R_{ct} ($\Omega.cm^2$)	30	170	1 300	80	85	110

Another noticeable change and which seems essential, concerns the impedance of the positive electrode after a storage at high voltage with GA additive (experimentally, for the sample after 14 days of storage, Figure 8e): it is considerably lower (150 $\Omega.cm^2$) than that observed without additive (2 500 $\Omega.cm^2$). Even if we could not have here, with the EIS technique, a visible signature of any protection of the positive electrode by the additive, we indirectly see that there is a beneficial change for the electrode/electrolyte interface. Actually, it leads to better performance upon long-term cycling, especially for the stability of the system to high voltages (up to 5V *vs.* Li). As evidenced by NMR and XPS, the chemical nature of the deposit on the surface of the positive electrode is different (less inorganic contributions) and its thickness is larger than that observed without the additive. However, from an impedance point of view, when the additive is used, the resulting passivation film is less resistive, probably due to a more porous morphology and/or a better ionic conductivity. The analysis of the semi-circle corresponding to the film gives interesting information about these last two points: for example, the parameter α associated to the film pseudo capacitance ($Z_{CPE\text{-}film} = \frac{1}{C(j\omega)^{\alpha}}$) is an indicator of the more or less porous nature of the film. Considering both EIS

spectra, obtained after the 30th cycle, with (Figure 8e) and without (Figure 8b) additive into the electrolyte respectively, the parameter α is closer to 1 when GA additive is used, indicating that the passivation film is more dense/homogeneous in that case. Since its thickness is larger (XPS) but its resistance is lower (EIS), it suggests that this dense/homogeneous film formed in presence of GA additive is a better ionic conductor (charged organic polymer). Thus we would rather be here in presence of a Polymer Electrolyte Interface (PEI). Considering the electrochemical active surface area, S_{elec}, of the positive electrode ($S_{geometric} < S_{elec} < S_{specific}$ *i.e* $1.54 < S_{elec} < 49$ cm^2), the thickness of the passivation film (e < 5 nm, from XPS results) and the resistance R_f and capicitance C_f associated after the 30th cycle (Figure 8b), an estimation of both the minimal ionic conductivity, σ_{ionic}, and permittivity, ε_r, of this layer could be proposed.[32]

$\sigma_{ionic} = \frac{1}{R_f} \times \frac{e}{S} \geq 10^{-9}$ S.cm^{-1} and $\varepsilon_r = \frac{C_f}{\varepsilon_0} \times \frac{e}{S} \geq 10$, which is actually consistent with a PEI layer.[33,34,35,36,37,38]

The use of GA additive clearly allows switching to a different degradation mechanism in which the decomposition of the electrolyte lithiated salt is hindered and the formation of a mostly organic passivation layer occurs. Moreover, this mechanism involves the transformation or degradation of the additive molecules. When the additive is used, the amount of Li is lower but still increases after more than 100 cycles. It seems then unlikely that all the lithiated species are located at the same distance from the active material. The quite stable FWHM observed by NMR along an extended cycling suggests a more homogenous distribution of the lithiated species in the dominantly organic matrix. Both XPS and NMR chemical information, together with EIS electrical recordings, support a more covering/homogenous and ionically conducting surface film on the positive electrode when GA is used as additive.

3.4. LTO electrode/electrolyte interface:

3.4.1. XPS:

Figures 10a and 10b show the O 1s and C 1s spectra of the LTO negative electrode with 2% of additive for the following samples: starting electrode, and after the first, the 30th and the 118th cycles, and after 14 days of storage in charged state before discharge.

The O 1s spectrum of the starting LTO electrode displays a narrow peak at 529.9 eV which is characteristic of O^{2-} anions of the crystalline network. The other peaks are assigned to adsorbed species at the surface.

Upon cycling, when 2% of GA is used in the electrolyte we can observe a significant deposition process of new oxygenated species (different from those observed without additive [9]) at the surface of the electrode. This effect is even stronger than at the surface of the positive electrode. As soon as the first cycle is achieved, the signature of the electrode material is no more the main peak of the spectrum. After 118 cycles it becomes very weak, showing that the covering process is very important. It is worth noting that the O 1s signature of the deposited species at the surface of the LTO electrode is different from that of the deposited species at the surface of the positive electrode. Therefore, different degradation mechanisms take place at both electrodes surfaces.

As for the positive electrode, the C 1s spectrum of the starting LTO negative electrode shown in Figure 10b consists of the peaks of conductive carbon and PVdF. Upon cycling, the deposition process of carbonaceous species at the surface of the electrode is quite significant and new carbon environments can be evidenced. In particular, the characteristic signature of O=C–O organic functions is observed. The covering process of the conductive carbon is displayed by the decrease of the intensity of the peak at 284 eV. Quantitative data for the LTO electrode after 118 cycles without and with 2% of additive are given in Table 2.

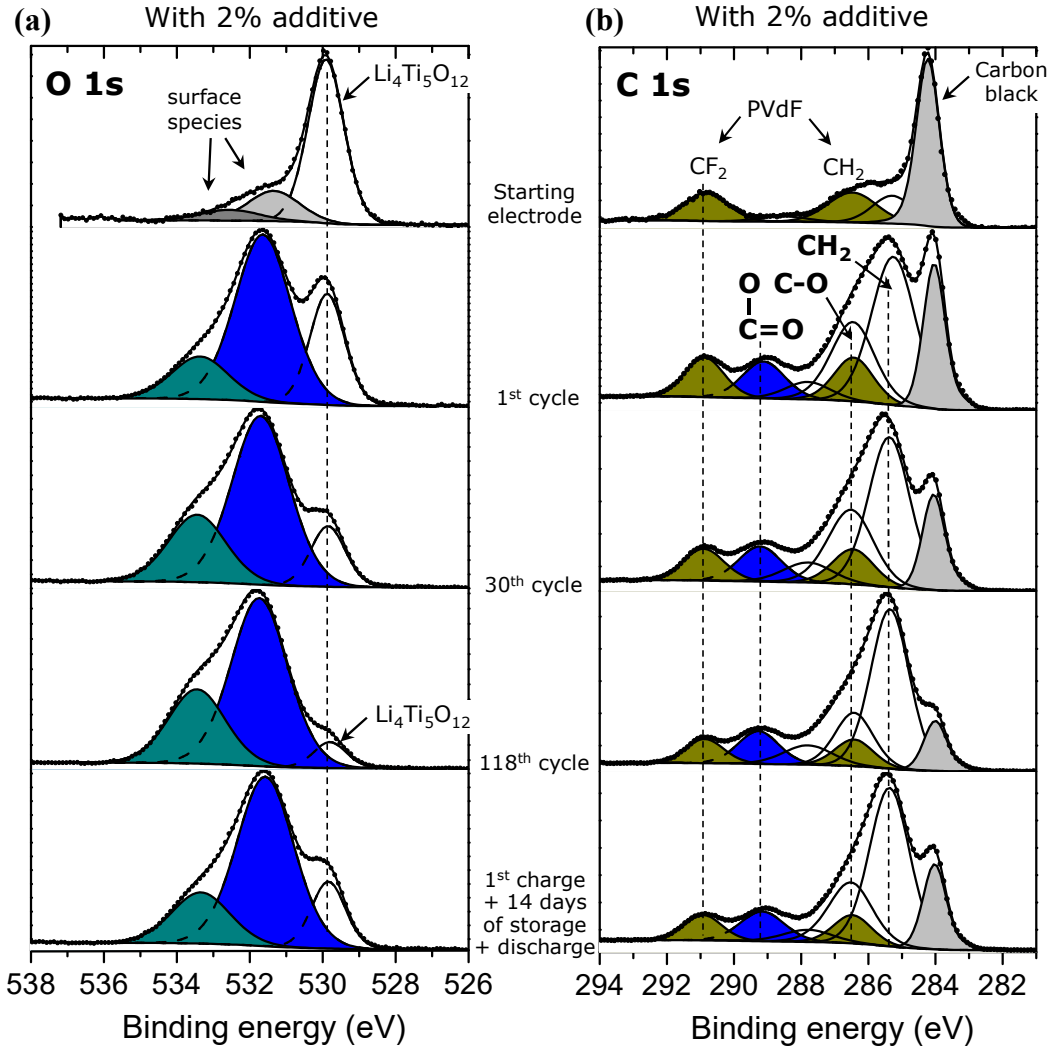

Figure 10: **(a)** O 1s and **(b)** C 1s spectra of the LTO negative electrode with 2% of GA: starting electrode, 1st, 30th and 118th cycles, and after 14 days of storage in charged state before discharge.

After 118 cycles with the additive, the amount of additional oxygen and carbon deposited at the surface of the electrode, corresponding to the organic species resulting from degradation of the additive accounts for more than 60 % of the composition of the surface (in the 5 nm thick layer analysed by XPS). Without the additive the amount of inorganic species is rather large, with about 13 % of LiF and 2 % of phosphorus assigned to phosphates for example. With 2% of GA in the electrolyte, the amount of LiF is about 5-6 % and the amount

of phosphorus about 0.5 %. Therefore, as for the positive electrode, the use of the additive results in a significant decrease of the proportion of inorganic species in the passivation layer of the negative electrode. It is also worth noting that manganese can be detected at the surface of the LTO negative electrode after 118 cycles (see Table 2).

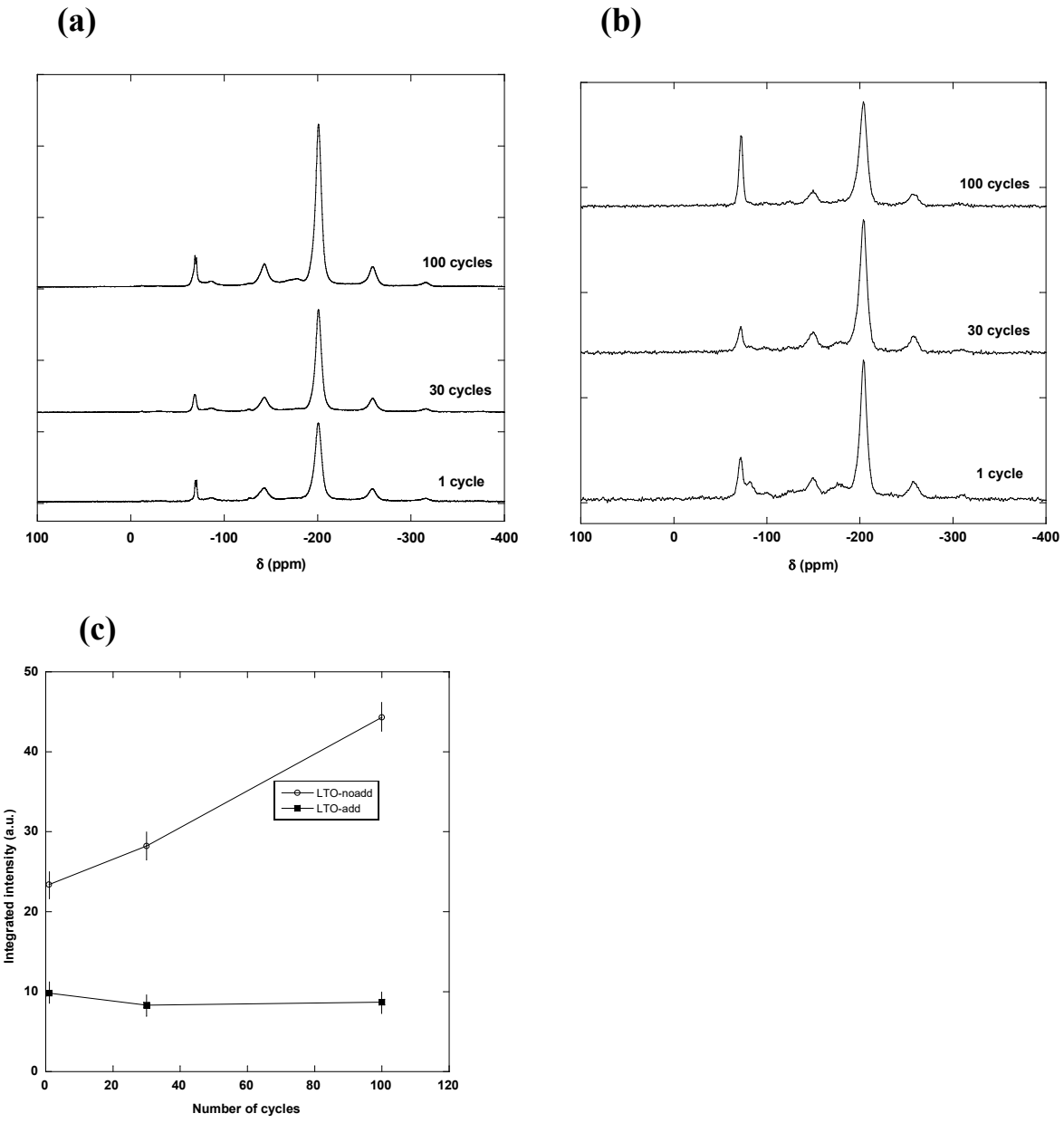

Figure 11: Normalized ^{19}F MAS NMR spectra of LTO negative electrodes: **(a)** without additive and **(b)** with 2% of GA. **(c)** Evolution of the normalized integrated intensities of ^{19}F MAS NMR spectra.

3.4.2. ^{19}F NMR:

These results are supported by ^{19}F NMR performed on CMC-based LTO electrodes, as shown in Figure 11. ^{19}F NMR normalized spectra of the negative electrode material after 1, 30 and 100 cycles display one main contribution at -205 ppm and a smaller second contribution at -72 ppm, assigned to LiF and $LiPF_6$, respectively (Figure 11a and 11b).[39] After one cycle, fluorine quantification (Figure 11c) shows that the amount of detected fluorine when no additive is used, is more than twice the amount detected when GA is present in the electrolyte. In addition, with 2% of additive, the amount of fluorine is kept very stable along the electrochemical cycling whereas a significant increase can be measured in absence of additive.

3.4.3. EIS:

The LTO electrode/electrolyte interface was also checked by EIS. The results are presented in Figure 12 and the corresponding values of global resistance Z', film resistance R_f and charge transfer resistance R_{ct} are given in Table 4.

As previously reported,[9] for the negative electrode in common electrolyte (without additive) a classic mechanism of electrochemical insertion (Randles type, Figure 9c) is observed from the early cycles of charge-discharge (with small variation of the charge transfer resistance, R_{ct}, from 20 to 10 $\Omega.cm^2$, Figure 12a). Then, upon cycling (Figure 12b), the increase of the global impedance results in a more depressed semi-circle at high frequency so that it could be possible to deconvoluate this first semi-circle in two intricate semi-circles with very close characteristic frequencies (both phenomena should have very close time constants).

In that case, it would be possible to fit diagrams with a film formation mechanism corresponding to a moderate resistive surface passivation of the electrode. This covering process is consistent with the observations enlighten by XPS and NMR and we can also notice, by EIS, the gradual increase of the surface covering (but still limited in terms of electrical resistance contribution, $R_{film} < 30\ \Omega.cm^2$). At that side of the battery, without

additive the deposit consists in a great amount of lithiated inorganic species (see XPS, NMR section), in contrast to what happens at the positive electrode, with the degradation of the electrolyte (given birth to mostly organic species). A Solid Electrolyte Interface (SEI) is thus observed on the surface of the negative LTO electrode, in conventional electrolyte, when associated to positive LNM electrode.

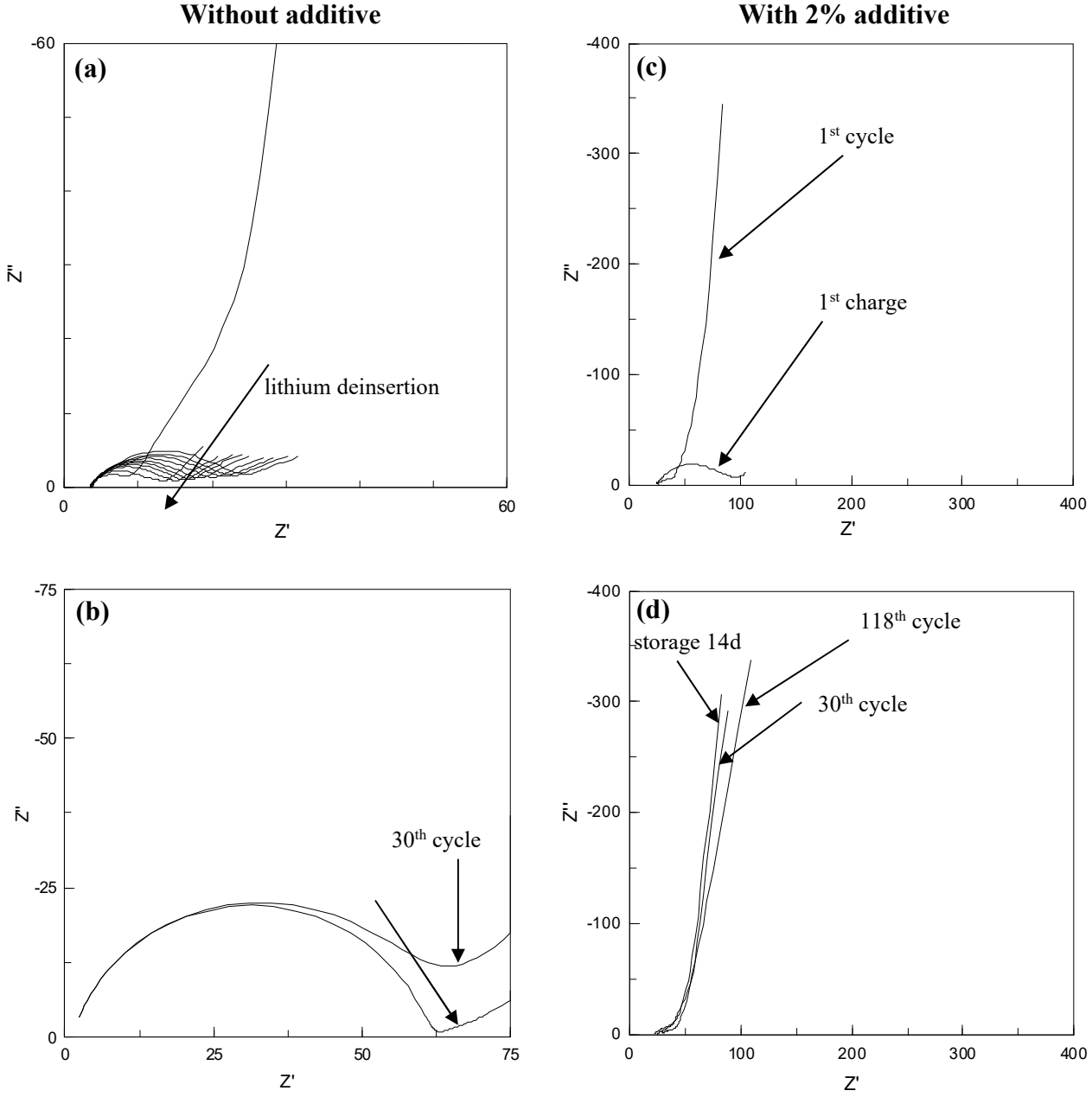

Figure 12: EIS diagrams of the LTO negative electrode: **(a)** evolution during lithium deinsertion (cell discharge after a first charge, without additive), **(b)** after 30 cycles and after 14 days of storage in charged state before discharge (without additive), **(c)** after the first charge and the first discharge (1st cycle) with 2% of GA, and **(d)** after 30 and 118 cycles and after 14 days of storage (with 2% of GA).

Table 4: LTO negative electrode. Resistance values ($\Omega.cm^2$) obtained from the EIS diagrams presented in Figure 12 with and without additive: global resistance Z', film resistance R_f and charge transfer resistance R_{ct}.

LTO electrode	Without additive			With 2% additive		
	30 cycles	118 cycles	Storage 14 days	30 cycles	118 cycles	Storage 14 days
Global resistance Z' ($\Omega.cm^2$)	80	100	75	40	45	45
Film resistance R_f ($\Omega.cm^2$)	20	28	18	25	30	25
Charge transfer resistance R_{ct} ($\Omega.cm^2$)	60	70	60	15	15	20

After the addition of 2% GA additive, the first process at the negative electrode is different, compared to what was observed in standard electrolyte. The previously claimed mechanism (conventional simple electrochemical insertion, with a decrease of the impedance during first charge) is now different (the impedance diagram exhibits 2 well defined semi-circles and the value of the impedance is 3 times larger, around 100 $\Omega.cm^2$), suggesting a greater passivation of the electrode surface at the beginning (1st charge, Figure 12c). However, it can be seen that this global impedance rapidly decreases since, after the 1st cycle, its value becomes close to that observed during the first cycles in standard electrolyte (around 30 $\Omega.cm^2$) and is stable upon cycling (after 30, 118 cycles or after storage during 14 days) (Figure 12d). From an impedance point of view, a severe transformation of the interface takes place during the first cycle (charge and discharge) since the total impedance of the negative electrode/electrolyte interface becomes quickly as small as in standard electrolyte whereas it starts much higher.

4. Conclusion

In this work, we have investigated the efficiency of GA additive to improve the electrochemical performances of LNM/LTO cells. We showed that GA allows a decrease of the capacity fading upon cycling (15% instead of 25% after ~120 cycles) and a decrease of the self-discharge for a battery maintained in charged state for two weeks (16% instead of 28%). We focused our investigation on electrode/electrolyte interfaces and we evidenced that addition of 2% of GA in the electrolyte results in a significant decrease of the amount of $LiPF_6$ salt decomposition products in the passivation film at the two electrodes surfaces (less lithium and phosphorus was detected). On the other hand, a much thicker passivation film is deposited at both electrodes, which is mainly composed of organic species ensuing from decomposition products of the GA additive. Therefore, it is proven that the additive actually produces a protective film at the surface of the electrodes. Especially at the LNM positive electrode, it reduces the electrode/electrolyte reactivity due to the very high potential reached at the end of charge (5V *vs.* Li). Impedance measurements have shown that, although the passivation film is much thicker with 2% of additive, it is less resistive and this is due to a better ionic conductivity. In this way, the passivation film behaves like a Polymer Electrolyte Interface (PEI). The results of this work show us that efficient solutions can be found with electrolyte additives to address performance and safety concerns encountered with high voltage spinel Li-ion batteries, to make them marketable for future applications.

Acknowledgments

The authors thank ANR (French National Research Agency) Stock-E program (ANR-08-STOCK-E-05) for financial support.

Supporting information

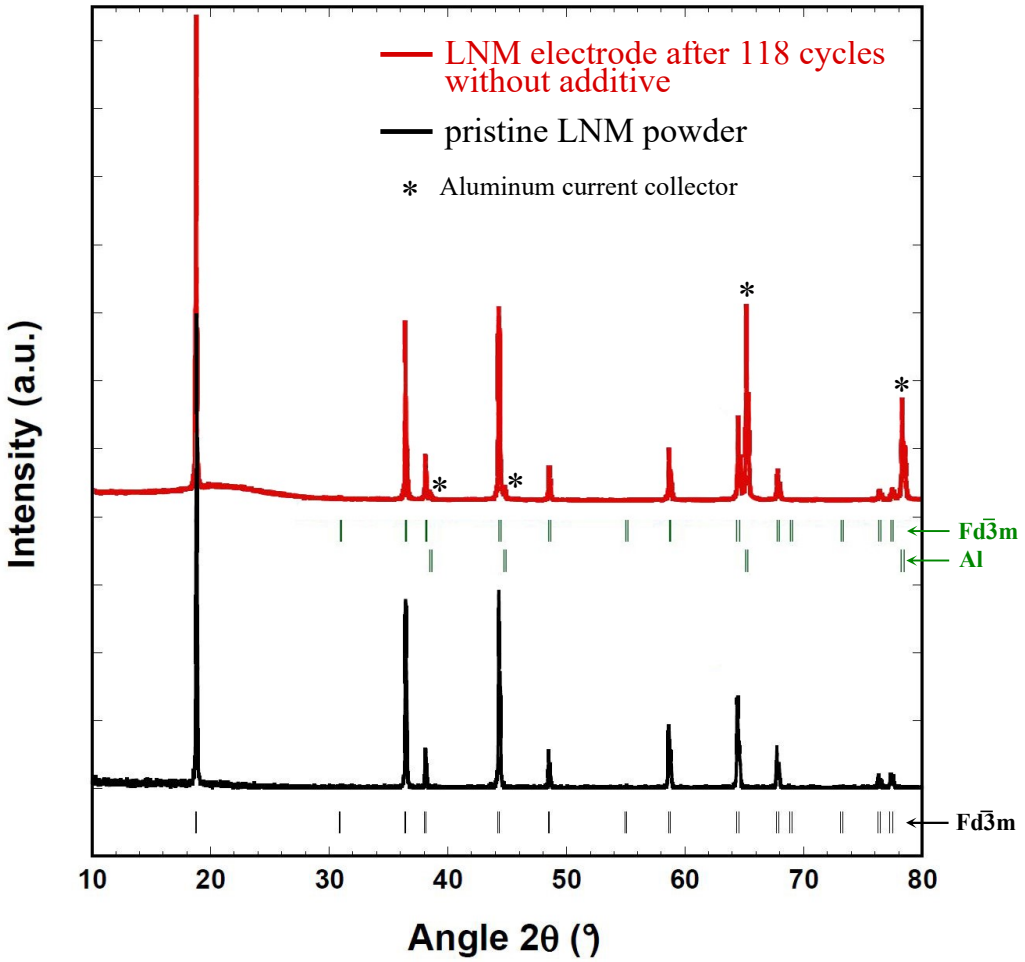

Figure S1: X-ray Diffraction patterns (Cu Kα radiation) of the $LiMn_{1.6}Ni_{0.4}O_4$ (LNM) pristine powder (black) and of the composite electrode (red) after 118 cycles of a LNM/LTO cell between 1.5 and 3.5 V at 20°C and a C/5 rate (without additive). No structural changes can be evidenced after cycling.

Appendix : *Kinetics equations for the electro-adsorption model*

From the electrochemical equations (1), (2) and (3), corresponding to elementary processes, we can deduce the following kinetics expressions.

The faradic current is defined by:

$$I_F = -FS\Gamma\left[k_c\theta - k_a(1-\theta)C_0\right] \tag{4}$$

with

$$k_c = k^0 \exp\left[\frac{-\alpha nF}{RT}(E - E^0)\right]$$

$$k_a = k^0 \exp\left[\frac{(1-\alpha)nF}{RT}(E - E^0)\right]$$

The occupied sites with adsorbed species are described by:

$$\frac{d\theta}{dt} = kC_{el}(1-\theta) - k_c\theta + k_a(1-\theta)C_0 = \frac{I_F}{FS\Gamma} + kC_{el}(1-\theta) \tag{5}$$

And the diffusion phenomenon satisfies to the Fick's laws :

$$-D_{Li}\frac{\partial C(x)}{\partial x} = \Phi = -k_c\Gamma\theta + k_a\Gamma(1-\theta)C_0 \tag{6}$$

$$\frac{\partial C(x)}{dt} = D_{Li}\frac{\partial^2 C(x)}{\partial x^2} \tag{7}$$

with these boundary conditions:

x = 0 corresponds to $C(0) = C_0$

and x = δ (diffusion layer thickness) corresponds to $C(\delta) = C$.

The linearization of the above expressions and the use of the Laplace's transform leads to:

From (5) : $$\overline{\Delta\theta}\, j\omega = \frac{\overline{\Delta I_F}}{FS\Gamma} + k(1-\theta)\overline{\Delta C_{el}} - kC_{el}\overline{\Delta\theta} \tag{8}$$

The electrolyte solution is enough concentrated (generally 1 $mol.L^{-1}$) to assume that C_{el} is constant with time, so we can simplify equation (8):

$$C_{el} = cst \Rightarrow \overline{\Delta C_{el}} = 0 \Rightarrow \overline{\Delta I_F} = FS\Gamma(j\omega + kC_{el})\overline{\Delta\theta} \tag{9}$$

From (6) and (7) : $\overline{\Delta C} = -T\overline{\Delta\Phi}$ with $T = \dfrac{th\left(\delta\sqrt{\dfrac{j\omega}{D_{Li}}}\right)}{\sqrt{j\omega D_{Li}}}$ so that we can write

$$\overline{\Delta C} = -\frac{T}{\left[1 + Tk_a\Gamma(1-\theta)\right]}\left\{\left(-k_c\Gamma - k_a\Gamma C_0\right)\overline{\Delta\theta} + \left[-b_c k_c\Gamma\theta + b_a k_a\Gamma(1-\theta)C_0\right]\overline{\Delta E}\right\} \tag{10}$$

But we know that : $\overline{\Delta I_F} = \left(\frac{\partial I_F}{\partial E}\right)_{\theta,C} \overline{\Delta E} + \left(\frac{\partial I_F}{\partial \theta}\right)_{E,C} \overline{\Delta \theta} + \left(\frac{\partial I_F}{\partial C}\right)_{\theta,E} \overline{\Delta C}$ (11)

with $\frac{\overline{\Delta E}}{\overline{\Delta I_F}} = Z_F$;

and $\left(\frac{\partial I_F}{\partial E}\right)_{\theta,C} = \frac{1}{R_{ct}}$ where R_{ct} symbolise the charge transfer resistance ;

So, finally, we can determine the faradic impedance (12):

$$Z_F = \frac{1 + \frac{k_c + k_a C_0}{j\omega + kC_{el}} + \frac{Tk_a(1-\theta)\Gamma(-k_c - k_a C_0)}{[1 + Tk_a\Gamma(1-\theta)](j\omega + kC_{el})}}{\frac{1}{R_{ct}}\left[\frac{1}{1 + Tk_a\Gamma(1-\theta)}\right]} = R_{ct} + R_{ct}Tk_a\Gamma(1-\theta) + \frac{R_{ct}(k_c + k_a C_0)}{j\omega + kC_{el}}$$

The faradic impedance is composed of three impedances in series: $Z_F = R_{ct} + Z_w + Z_1$

where Z_W is the Warburg diffusion impedance, here $Z_w = R_{ct}Tk_a\Gamma(1-\theta)$.

Z_1 is more complex but is actually composed of two other impedances in parallel:

$$\frac{1}{Z_1} = \frac{j\omega}{R_{ct}(k_c + k_a C_0)} + \frac{kC_{el}}{R_{ct}(k_c + k_a C_0)} = j\omega C_{ads} + \frac{1}{R_{ads}}$$

where

$R_{ads} = \frac{R_{ct}(k_c + k_a C_0)}{kC_{el}}$ and $C_{ads} = \frac{1}{R_{ct}(k_c + k_a C_0)}$.

Finally, we can build an electrical equivalent circuit for this electro-adsorption model (Figure 9a).

References

1 Goodenough, J. B.; Kim, Y., Challenges for Rechargeable Li Batteries. *Chem. Mater.* **2010**, *22,* 587-603.

2 Ferg, E.; Gummow, R.; de Kock , J. A.; Thackeray, M. M., Spinel Anodes for Lithium-Ion Batteries. *J. Electrochem. Soc.* **1994,** *141*, L147-L150.

3 Ohzuku, T.; Ueda, A.; Yamamoto, N., Zero-Strain Insertion Material of $Li[Li_{1/3}Ti_{5/3}]O_4$ for Rechargeable Lithium Cells. *J. Electrochem. Soc.* **1995,** *142*, 1431-1435.

4 Jansen, A.; Kahaian, A. J.; Kepler, K. D.; Nelson, P. A.; Amine, K.; Dees, D. W.; Vissers, D. R.; Thackeray, M. M., Development of a High-Power Lithium-Ion Battery. *J. Power Sources* **1999**, *81-82*, 902-905

5 Amine, K.; Tukamoto, H.; Yasuda, H.; Fujita, Y., Preparation and Electrochemical Investigation of $LiMn_{2-x}Me_xO_4$ (Me: Ni, Fe, and x = 0.5, 1) Cathode Materials for Secondary Lithium Batteries. *J. Power Sources* **1997**, *68*, 604-608.

6 Zhong, Q.; Bonakdarpour, A.; Zhang, M.; Gao, Y.; Dahn, J. R., Synthesis and Electrochemistry of $LiNi_xMn_{2-x}O_4$. *J. Electrochem. Soc.* **1997,** *144*, 205-213.

7 Patoux, S.; Daniel, L.; Bourbon, C.; Lignier, H.; Pagano, C.; Le Cras, F.; Jouanneau, S.; Martinet, S., High Voltage Spinel Oxides for Li-Ion Batteries: From the Material Research to the Application. *J. Power Sources* **2009**,*189*, 344-352.

8 Xu, K., Electrolytes and Interphasial Chemistry in Li Ion Devices. *Energies* **2010**, *3*, 135-154.

9 Dedryvère, R.; Foix, D.; Franger, S.; Patoux, S.; Daniel, L.; Gonbeau, D., Electrode/Electrolyte Interface Reactivity in High-Voltage Spinel $LiMn_{1.6}Ni_{0.4}O_4/Li_4Ti_5O_{12}$ Lithium-Ion Battery. *J. Phys. Chem. C* **2010**, *114*, 10999-

11008.

10 Wang, Z.; Dupré, N.; Lajaunie, L.; Moreau, P.; Martin, J. F.; Boutafa, L.; Patoux, S.; Guyomard, D., Effect of Glutaric Anhydride Additive on the $LiNi_{0.4}Mn_{1.6}O_4$ Electrode/Electrolyte Interface Evolution: a MAS NMR and TEM/EELS Study. *J. Power Sources* **2012**, *215*, 170-178.

11 Aurbach, D.; Levi, M. D.; Levi, E.; Teller, H.; Markovsky,B.; Salitra, G.; Heider, L., Common Electroanalytical Behavior of Li Intercalation Processes into Graphite and Transition Metal Oxides. *J. Electrochem. Soc.* **1998**, *145*, 3024-3034.

12 Hu, M.; Pang, X.; Zhou, Z., Recent Progress in High-Voltage Lithium Ion Batteries. *J. Power Sources* **2013**, *237*, 229-242.

13 Xu, K.; Zhang, S. S.; Lee, U.; Allen, J. L.; Jow, T. R., LiBOB: Is It an Alternative Salt for Lithium Ion Chemistry ? *J. Power Sources* **2005**, *146*, 79-85.

14 Santee, S.; Xiao, A.; Yang, L.; Gnanaraj, J.; Lucht ,B. L., Effect of Combinations of Additives on the Performance of Lithium Ion Batteries. *J. Power Sources* **2009**, *194*, 1053-1060.

15 Li, W.; Xiao, A.; Lucht, B. L.; Smart, M. C.; Ratnakumar ,B. V., Surface Analysis of Electrodes from Cells Containing Electrolytes with Stabilizing Additives Exposed to High Temperature. *J. Electrochem. Soc.* **2008**, *155*, A648-A657

16 Buqa, H.; Golob, P.; Winter, M.; Besenhard, J. O., Modified Carbons for Improved Anodes in Lithium Ion Cells. *J. Power Sources* **2001**, *97-98*, 122-125.

17 Tarnopolskiy, V.; Kalhoff, J.; Nadherna, M.; Bresser, D.; Picard, L.; Fabre, F.; Rey, M.; Passerini, S., Beneficial Influence of Succinic Anhydride as Electrolyte Additive on the Self-Discharge of 5 V $LiNi_{0.4}Mn_{1.6}O_4$ Cathodes. *J. Power Sources* **2013**, *236*, 39-46.

18 Han, G. B.; Ryou, M.-H.; Cho, K. Y.; Lee, Y. M.; Park, J.-K., Effect of Succinic Anhydride as an Alectrolyte Additive on Electrochemical Characteristics of Silicon

Thin-Film Electrode. *J. Power Sources* **2010**, *195*, 3709–3714.

19 Grey, C. P.; Dupré, N., NMR Studies of Cathode Materials for Lithium-Ion Rechargeable Batteries. *Chem. Rev.* **2004**, *104*, 4493-4512.

20 Bekaert, E.; Robert, F.; Lippens, P. E.; Ménétrier, M., ^{7}Li NMR Knight Shifts in Li−Sn Compounds: MAS NMR Measurements and Correlation with DFT Calculations. *J. Phys. Chem. C* **2010**, *114*, 6749–6754.

21 Ménétrier, M.; Saadoune, I.; Levasseur, S.; Delmas, C., The Insulator-Metal Transition upon Lithium Deintercalation from $LiCoO_2$: Electronic Properties and ^{7}Li NMR Study. *J. Mater. Chem.* **1999**, *9*, 1135-1140.

22 Dupré, N.; Martin, J. F.; Yamada, A.; Kanno, R.; Guyomard, D., Detection of Surface Layers Using ^{7}Li MAS NMR. *J. Mater. Chem.* **2008**, *18*, 4266-4273.

23 Meyer, B. M.; Leifer, N.; Sakamoto, S.; Greenbaum, S. G.; Grey, C. P., High Field Multinuclear NMR Investigation of the SEI Layer in Lithium Rechargeable Batteries. *Electrochem. Solid-State Lett.* **2005**, *8*, A145-A148.

24 Ménétrier, M.; Vaysse, C.; Croguennec, L.; Delmas, C.; Jordy, C.; Bonhomme, F.; Biensan, P., ^{7}Li and ^{1}H MAS NMR Observation of Interphase Layers on Lithium Nickel Oxide Based Positive Electrodes of Lithium-Ion Batteries. *Electrochem. Solid-State Lett.* **2004**, *7*, A140-A143.

25 Jouanneau, S.; Le Cras, F.; Bourbon, C.; Lignier, H., CEA, Patent # WO2006/027449.

26 Shirley, D. A., High-Resolution X-Ray Photoemission Spectrum of the Valence Bands of Gold. *Phys. Rev. B* **1972**, *5*, 4709-4714.

27 Scofield, J., H. Hartree-Slater Subshell Photoionization Cross-Sections at 1254 and 1487 eV. *J. Electron Spectrosc. Relat. Phenom.* **1976**, *8*, 129-137.

28 Massiot, D., http://nmr.cemhti.cnrs-orleans.fr/dmfit/

29 Van Veenendaal, M. A.; Heskes, H.; Sawatzky, G. A., Strong Nonlocal Contributions to

Cu 2p Photoelectron Spectroscopy. *Phys. Rev. B* **1993**, *47*, 11462-11469.

30 Van Veenendaal, M. A.; Sawatzky, G. A., Nonlocal Screening Effects in 2p X-Ray Photoemission Spectroscopy Core-Level Line Shapes of Transition Metal Compounds. *Phys. Rev. Lett.* **1993**, *70*, 2459-2462.

31 Dahéron, L.; Dedryvère, R.; Martinez, H.; Ménétrier, M.; Delmas, C.; Gonbeau, D., Electron Transfer Mechanisms upon Lithium Deintercalation from $LiCoO_2$ to CoO_2 Investigated by XPS. *Chem. Mater.* **2008**, *20,* 583-590.

32 Franger, S.; Bach, S.; Farcy, J.; Pereira-Ramos, J.-P.; Baffier, N., An Electrochemical Impedance Spectroscopy Study of New Lithiated Manganese Oxides for 3V Application in Rechargeable Li-Batteries. *Electrochim. Acta* **2003**, *48*, 891-900.

33 Sorensen, P. R.; Jacobsen, T., Conductivity, Charge Transfer and Transport Number – an AC-Investigation of the Polymer Electrolyte LiSCN-Poly(ethyleneoxide). *Electrochim. Acta* **1982**, *27*, 1671-1675.

34 Froment, M.; Garreau, M.; Thevenin, J.; Warin, D., Composition of Passivating Layers Formed on Lithium Electrodes in Lithium Perchlorate and Propylene Carbonate Solutions. *J. Micro. Spectro. Electron.* **1979**, *4*, 111-114.

35 Thevenin, J.; Muller, R. H., Impedance of Lithium Electrodes in a Propylene Carbonate Electrolyte. *J. Electrochem. Soc.* **1987**, *134*, 273-280.

36 Robitaille, C. D.; Fauteux, D., Phase Diagrams and Conductivity Characterization of Some PEO - Li_X Electrolytes. *J. Electrochem. Soc.* **1986**, *133*, 315-325.

37 Pals, C. R.; Newman, J., Thermal Modeling of the Lithium/Polymer Battery: I . Discharge Behavior of a Single Cell. *J. Electrochem. Soc.* **1995**, *142*, 3274-3281.

38 Wetton, R. E.; James, D. B.; Warner, F. P., in "Ions in Polymer", Eds. A. Eisenberg **1980**.

39 Plakhotnyk, A. V.; Ernst, L.; Schmutzler, R., Hydrolysis in the System $LiPF_6$-Propylene Carbonate-Dimethyl Carbonate-H_2O. *J. Fluorine Chem.* **2005**, *126*, 27-31.